Detailing the optimality of photosynthesis in cyanobacteria through systems biology analysis

Juan Nogales[1], Steinn Gudmundsson, Eric M. Knight, Bernhard O. Palsson, and Ines Thiele[2]

Center for Systems Biology, University of Iceland, 101 Reykjavik, Iceland

Edited by Robert Haselkorn, University of Chicago, Chicago, IL, and approved December 28, 2011 (received for review November 8, 2011)

Photosynthesis has recently gained considerable attention for its potential role in the development of renewable energy sources. Optimizing photosynthetic organisms for biomass or biofuel production will therefore require a systems understanding of photosynthetic processes. We reconstructed a high-quality genome-scale metabolic network for *Synechocystis* sp. PCC6803 that describes key photosynthetic processes in mechanistic detail. We performed an exhaustive in silico analysis of the reconstructed photosynthetic process under different light and inorganic carbon (*Ci*) conditions as well as under genetic perturbations. Our key results include the following. (*i*) We identified two main states of the photosynthetic apparatus: a *Ci*-limited state and a light-limited state. (*ii*) We discovered nine alternative electron flow pathways that assist the photosynthetic linear electron flow in optimizing the photosynthesis performance. (*iii*) A high degree of cooperativity between alternative pathways was found to be critical for optimal autotrophic metabolism. Although pathways with high photosynthetic yield exist for optimizing growth under suboptimal light conditions, pathways with low photosynthetic yield guarantee optimal growth under excessive light or *Ci* limitation. (*iv*) Photorespiration was found to be essential for the optimal photosynthetic process, clarifying its role in high-light acclimation. Finally, (*v*) an extremely high photosynthetic robustness drives the optimal autotrophic metabolism at the expense of metabolic versatility and robustness. The results and modeling approach presented here may promote a better understanding of the photosynthetic process. They can also guide bioengineering projects toward optimal biofuel production in photosynthetic organisms.

constraint-based modeling | photobioenergetic | metabolic engineering | biosustainability | metabolic robustness

The recent emphasis on biosustainability has brought attention to photosynthetic microorganisms. Microphototrophs, including cyanobacteria, represent efficient biological systems for producing biomass from inorganic carbon (*Ci*) and high-value products such as carotenoids, and they are also viewed as a potential source of biofuel (1, 2). On the other hand, photosynthesis is an inherently inefficient process, and photoautotrophic growth is limited by environmental perturbations (3). The success of future light-driven bioengineering approaches requires a systems understanding of the photosynthetic processes, including their bioenergetics and robustness.

Optimal photosynthetic performance requires fine-tuning the light/energy conversion by the photosystems and metabolic reactions, with the ATP/NADPH ratio being a particularly important parameter (4, 5). Carbon dioxide (CO_2) fixation through the Calvin cycle is the main ATP and NADPH sink in the autotrophic metabolism, requiring an ATP/NADPH ratio of 1.5. Because the photosynthetic linear electron flow (LEF) pathway generates an ATP/NADPH ratio of 1.28, additional ATP is needed (4, 5). Phototrophs have developed a large arsenal of alternate electron flow (AEF) pathways, which assist in modulating the ATP/NADPH ratio as a function of the metabolic demand. Although the in vivo physiological roles of the AEF pathways are not completely known because of their cyclical nature, they are believed to work cooperatively with LEF (4, 6). The development of genome-scale metabolic models is therefore desirable for systematic understanding of the photosynthetic process (2, 4). To date, analysis of photosynthetic processes at the genome-scale has received limited attention (7).

The cyanobacterium *Synechocystis* sp. PCC6803, henceforth called *Synechocystis*, is a model photosynthetic prokaryotic organism capable of growing phototrophically because of oxygenic photosynthesis and heterotrophically at the expense of reduced carbon sources in the dark. These features make *Synechocystis* an interesting microorganism for biotechnology applications. Although several central-metabolic and genome-scale reconstructions are available for *Synechocystis* (8–12), they do not describe photosynthetic and heterotrophic metabolism in detail. Moreover, pathways relevant for biotechnological endeavors, such as the biosynthesis of lipids and photosynthetic pigments, are currently poorly represented. To fill these gaps, we reconstructed a high-quality genome-scale metabolic network of *Synechocystis* named *i*JN678. Here we describe *i*JN678 and the properties of the metabolic network it represents.

Results

Reconstruction Content, Enhancements, and Validation. We assembled a genome-scale metabolic reconstruction of *Synechocystis* based on available genomic and biochemical data by using an established reconstruction protocol (13). The final reconstruction, *i*JN678, contains 678 genes, 863 metabolic and transport reactions, and 795 nonunique metabolites, which are distributed over 54 subsystems and four different cellular compartments: extracellular, periplasm, cytoplasm, and thylakoid (*SI Appendix*, Table S1 and Dataset S1).

To enable systems analysis of the photosynthetic processes, an extensive effort was made to construct a complete and compartmentalized model of photosynthesis that exceeds previously published efforts in detail and coverage (8–11). The LEF reconstruction includes individual reactions for photosystem II (PSII), cytochrome b_6f (CytBF), photosystem I (PSI), and ferredoxin NADP$^+$ oxidoreductase (FNR), which were connected through plastoquinone (PQ), plastocyanin/cytochrome C (cytC), and ferredoxin, respectively (5). The AEF modeling includes the ferredoxin PQ reductase (FQR) and the NAD(P)H dehydrogenase complexes (14, 15), the aa3-type terminal oxidase (CYO), the PQ oxidase (CydBD), the MEHLER (16), and the hydrogenase (H2ase) (17) reactions. We additionally included the three photorespiration (PHOTOR) branches (18) and succinate dehydrogenase (SDH). The CYO, CydBD, and SDH reactions were also placed in the thylakoid membrane-enabling interaction between respiration and photosynthesis (19). The modeled photosynthetic apparatus is depicted in *SI Appendix*,

Author contributions: J.N., S.G., and I.T. designed research; J.N. and S.G. performed research; J.N., S.G., E.M.K., and B.O.P. contributed new reagents/analytic tools; J.N. and S.G. analyzed data; and J.N., S.G., E.M.K., B.O.P., and I.T. wrote the paper.

The authors declare no conflict of interest.

This article is a PNAS Direct Submission.

Freely available online through the PNAS open access option.

[1]Present address: Department of Bioengineering, University of California at San Diego, La Jolla, CA 92093.

[2]To whom correspondence should be addressed. E-mail: ines.thiele@gmail.com.

This article contains supporting information online at www.pnas.org/lookup/suppl/doi:10.1073/pnas.1117907109/-/DCSupplemental.

Fig. S1. The complete biosynthesis pathways for fatty acids, including ω-3 polyunsaturated fatty acids, and for photosynthetic-specific lipids were captured as well as the biosynthetic pathways for photosynthetic pigments, including chlorophyll *a*, phylloquinone, lycopene, β-carotenoids, zeaxanthin, echinenone, and α-, β-, γ- and δ-tocopherols. This level of detail allowed us to define an accurate biomass objective function (BOF) (Dataset S2). It also opens up the possibility for future biotechnology ventures to focus on the overproduction of these high-value compounds. Finally, the modeling of the heterotrophic metabolism was enhanced by including all transport reactions with genetic or physiological evidence (*SI Appendix*, Fig. S2). A detailed description of the major areas of enhancement of *i*JN678 was compared with published reconstructions (*SI Appendix*, Table S2).

Genome-scale reconstructions need to be validated by assessing their ability to compute physiological states (13). We validated *i*JN678 by comparing growth predictions with experimental values. The prediction error was less than 5% under mixotrophic and autotrophic conditions (*SI Appendix*, Table S3). Finally, the model predicted flux distributions, which correlated well with experimentally determined fluxes under the heterotrophic, mixotrophic, and autotrophic conditions (τ = 0.89, 0.92, and 0.96, respectively) (refs. 20 and 21; *SI Appendix*, Figs. S5–S7 and Dataset S3). A validated model can be used to characterize the metabolic states that underlie observed phenotypic functions.

Optimal Autotrophic Metabolism Requires the Contribution of Alternative Photosynthetic Electron Flow Pathways. We studied the photosynthetic process as a function of *Ci* and light availability. Maximal possible growth rates were computed under varying light conditions while maintaining a fixed *Ci* uptake rate (Fig. 1). We identified two unique states: (*i*) an initial state in which light, not *Ci*, was the growth-limiting factor [light-limited state (LLS)] and (*ii*) a final state in which *Ci* was growth-limiting instead of light [*Ci*-limited state (CLS)]. Under LLS, the fluxes through the LEF pathway, ATPase, and the HCO_3 uptake increased with light availability. The attainment of maximum *Ci* uptake [3.7 mmol·g dry wt (gDW)$^{-1}$·h^{-1}] marked the beginning of CLS, which was characterized by light excess and *Ci* limitation. The increasing light availability led to more photosynthetic activity and, thus, to higher levels of reducing equivalents (PSII, PSI, or FNR) and ATP (ATPase) (Fig. 1).

By constraining the AEF and PHOTOR pathways, we found that the balancing of the ATP/NADPH ratio and the prevention of internal overreduction were achieved by the reduction of an extra NO_3 (Fig. 1*A*). The excess of NH_4 produced was fixed via synthesis of cyanophycin, a cyanobacteria-specific nitrogen and carbon storage polymer, and led to a suboptimal growth rate. Under CLS, the high level of reducing equivalents produced exceeded the energy-dissipation capabilities of the NO_3 reduction pathway, and the model could not grow. The inclusion of PHOTOR in the simulation resulted in a suboptimal growth rate under CLS (Fig. 1*B*). This result suggests that PHOTOR could act as an energy-dissipation pathway under these conditions, which is in good agreement with the participation of PHOTOR in high-light acclimation (22).

When the growth rate was computed allowing one AEF at the time, we found that, in all cases, optimal growth rate was achieved. Under LLS, AEF pathways guaranteed optimal growth by consuming reducing equivalents and increasing the ATP levels (Fig. 1 *C*–*I*). The computed ATP/NADPH ratios were greater than 1.55 in all cases (Fig. 1*J*). They were higher than the ratio provided by LEF alone (i.e., 1.28) and agreed with the reported optimal requirement for CO_2 fixation (i.e., 1.5) (5). Under CLS, AEF pathways primarily acted as photoenergy-dissipation pathways by consuming reducing equivalents and dissipating more than 50% of available photons (hv_i/hv_o) (Fig. 1*J*).

Our analysis showed that the LEF pathway alone did not enable maximal growth under suboptimal light conditions but that the AEF pathways were also required, in agreement with previous observations (5, 6, 23). Furthermore, the results highlight

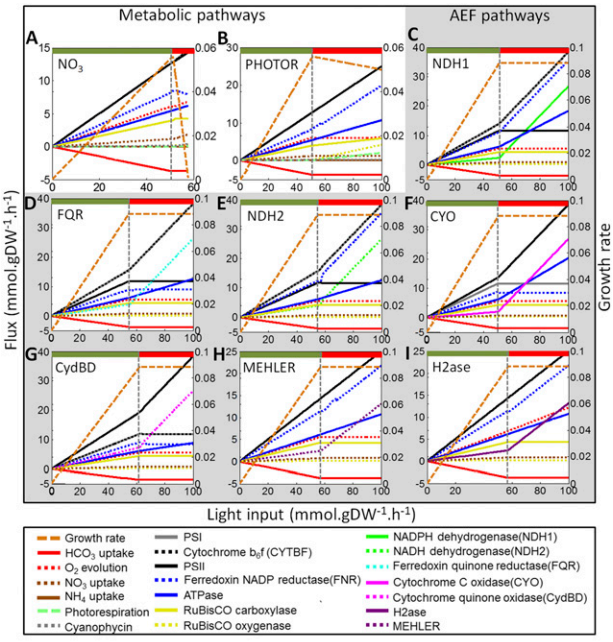

J

		CEF			PCEF		Auxiliary pathways		PHOTOR
		NDH1‡	NDH2	FQR	CydBD	CYO	H2ase	MEHLER	
LLS	Growth Rate (h^{-1})	0.051	0.048	0.048	0.042	0.052	0.046	0.046	-
	PSI/PSII	1.202	1.341	1.321	0.619	0.850	1.000	1.000	-
	ATP/NADPH	1.589	1.578	1.561	1.550	1.589	1.551	1.550	-
	Φ_{co2}(mol CO_2.mol hv^{-1})	0.072	0.068	0.068	0.059	0.073	0.065	0.065	-
	hv_i/hv_o(‰)	9.19	14.58	13.84	23.54	8.14	17.11	17.03	-
CLS	Growth Rate(h^{-1})	0.088	0.088	0.088	0.088	0.088	0.088	0.088	0.050
	PSI/PSII	3.283	3.283	3.209	0.305	0.305	1.000	1.000	1.000
	ATP/NADPH	4.710	3.243	3.179	2.264	5.200	2.706	2.689	1.343
	Φ_{co2}(mol CO_2.mol hv^{-1})	0.037	0.037	0.037	0.037	0.037	0.037	0.037	0.037
	hv_i/hv_o(‰)	53.3	53.3	52.5	53.3	53.3	52.5	52.2	19.1

Fig. 1. Impact of *Ci* (i.e., HCO_3^-) and light availability on the autotrophic metabolism of *Synechocystis*. Shown are the functional states found in the absence of AEF pathways and PHOTOR (*A*), the absence of AEF pathways allowing PHOTOR (*B*), and the presence of one AEF pathway (indicated by the caption in each diagram) (*C*–*I*). The growth rate (orange, right *y* axis) was computed under autotrophic conditions by using HCO_3^- as *Ci* source (uptake rate = 3.7 mmol·gDW^{-1}·h^{-1}) and NO_3 as nitrogen source (unconstrained uptake rate) as a function of light availability by varying the photon uptake rate from 0 to 100 mmol·gDW^{-1}·h^{-1} (*x* axis). The computed flux rates for each relevant reaction are shown (left *y* axis). The boundary between LLS (green) and CLS (red) states is shown by a vertical gray line. (*J*) Main photosynthetic and bioenergetics parameters yielded by the AEF pathways and PHOTOR. Light uptake rates of 30 and 100 mmol·gDW^{-1}·h^{-1} were taken as representative of the LLS (green) and CLS (red), respectively. The parameters from high and low photosynthetic-yield AEF pathways are shown in blue and pink, respectively. Because NDH-1$_3$, NDH-1$_4$, and NDH-1 exhibited identical parameters in both LLS and CLS, only NDH-1 is shown.

that growth under environmental perturbations, such as high light or *Ci* depletion, also highly depended on the AEF pathways and PHOTOR.

Quantification and Classification of Alternative Photosynthetic Pathways. Cyclic electron flow (CEF) around PSI has been suggested to be the main AEF pathway in phototrophs and to be primarily responsible for supplying the additional ATP required for CO_2 fixation (5, 6). We identified five CEF pathways assisting the LEF in ATP/NADPH balancing: Three pathways were involved in returning electrons to the PQ pool from NADPH (NDH-1, NDH-1$_3$, and NDH-1$_4$), and the NDH-2 and FQR pathways used NADH and reduced ferredoxin as electron donors, respectively (Figs. 1 *C*–*E* and 2). The flux across CEF pathways resulted in PSI/PSII ratios above 1.20, which agrees with theoretical estimates (Fig. 1*J*) (5).

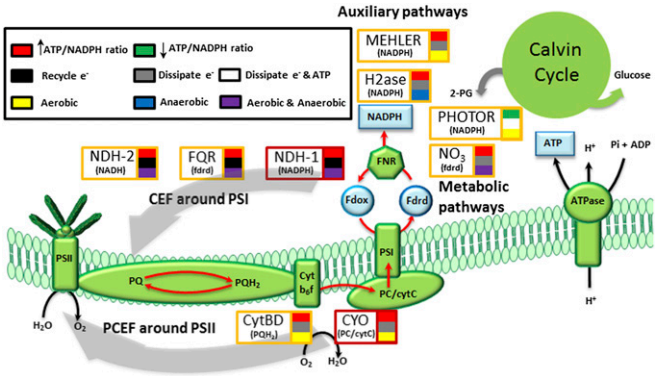

Fig. 2. Functional characterization of the alternative photosynthetic pathways involved in ATP/NADPH balancing and photoenergy dissipation. The LEF pathway (PSII, PQ pool, CytBF, PSI, and FNR), the ATPase, and the Calvin cycle are shown in green. The final products from LEF and photophosphorylation [reduced ferrodoxin (Fdrd), NADPH, and ATP] are shown in blue. The high and low light-yield pathways and their electron donors are shown with red and yellow boxes, respectively. Furthermore, the alternative pathways were color-coded based as shown based on their contribution to the ATP/NADPH ratio, the mechanism of dissipation, and by dependence on O_2 availability.

The computed quantum yield (Φ_{CO_2}, i.e., moles of photons absorbed per mole of CO_2 fixed) varied as a function of the used CEF pathways. The NDH-1–related pathways showed higher quantum yield (Φ_{CO_2} = 0.072) than NDH-2 and FQR did (Φ_{CO_2} = 0.068) (Fig. 1*J*). The Φ_{CO_2}, measured under light-limited conditions, is a standard measure of photosynthetic efficiency, with mean Φ_{CO_2} values of 0.052 for C_3 plants and 0.057 for the more efficient C_4 plants (24). Based on our computed Φ_{CO_2}, we suggest that CEF pathways are not equivalent. Using the arbitrary Φ_{CO_2} value of 0.070 as cutoff, we suggest that NDH-2 and FQR pathways are low photosynthetic-yield pathways, whereas NDH-1–related CEF pathways can be classified as high photosynthetic-yield pathways (Fig. 1*J*). Under CLS, a large increase in flux through the CEF pathways was predicted, which indirectly consumed more than 52% of available photons (Fig. 1*J*). Consequently, the PSI/PSII and ATP/NADPH ratios increased more than three- and fourfold, respectively (Fig. 1). These results are consistent with reports that light excess and low CO_2 levels induce CEF around PSI (6, 14).

The PQ oxidase CydBD and the terminal cytC oxidase CYO were identified as AEF pathways involved in a pseudocyclic electron flow (PCEF) around PSII (Fig. 2). Under LLS, the flow of electrons around PSII resulted in a PSI/PSII ratio of less than 1 but an optimal ATP/NADPH ratio (Fig. 1 *F*, *G*, and *J*). The CYO and CydBD pathways could be classified as high and low photosynthetic-yield pathways, respectively, based on the calculated Φ_{CO_2} values similar to CEF pathways (Fig. 1*J*). Under CLS, PCEF also enabled optimal growth by acting as an electron sink, indirectly consuming more than 53% of the available photons and preventing internal overreduction (Fig. 1 *F*, *G*, and *J*). In agreement with our in silico data, genetic evidence showed that, in the absence of PSI or under high-light conditions, terminal oxidases in *Synechocystis* used PSII-generated electrons and provided extra ATP levels (15, 25).

In addition to CEF and PCEF, our in silico analysis identified the NADPH-dependent reactions MEHLER (reduction of O_2) and H2ase as reactions assisting the LEF. These pathways yielded a PSI/PSII ratio of 1, low Φ_{CO_2} values, and reduced growth rates under LLS (Fig. 1 *H*–*J*). The difference between the H2ase and the MEHLER pathways was the O_2 evolution and larger flux through the H2ase pathway. Our analysis thus suggests that the H2ase and MEHLER reactions may be complementary low photosynthetic-yield systems whose activity depends on O_2 availability. Indeed, experimental evidence indicates that H2ase only operates in anaerobic or microaerobic conditions, whereas MEHLER pathways require aerobic conditions (17, 26).

In summary, our analysis suggests that *Synechocystis* has a large number of AEF pathways involved to preserve optimal photosynthetic processes under environmental perturbation, such as *Ci* or light availability (photosynthetic robustness). The quantitative analysis of photosynthetic parameters exhibited by *i*JN678 allowed us to classify these AEF pathways based on (*i*) photosynthetic yield, (*ii*) net contribution to the ATP/NADPH ratio, (*iii*) mechanisms used for ATP/NADPH balancing and/or energy dissipation, (*iv*) dependency on O_2 availability, and (*v*) LEF target components on which they acted (Fig. 2). This classification represents a valuable tool for better understanding how phototrophs might select among their large array of accessory photosynthetic pathways those that are best suited for efficient response to environmental perturbations.

PHOTOR Plays an Active Role as an ATP-Consuming Pathway Under CLS. PHOTOR recycles 2-phosphoglycolate, which is produced by the oxygenic reaction of ribulose-1,5-bisphosphate carboxylase/oxygenase (RuBisCO). This process leads to a net loss of carbons and reduces the efficiency of photosynthesis because one glyceraldehyde 3-phosphate molecule and one CO_2 molecule are produced from two 2-phosphoglycolate molecules. We found that PHOTOR was not active under LLS but that it enabled growth under CLS in absence of AEF (Fig. 1*B*). PHOTOR acted as an alternative energy-dissipation pathway under CLS, yielding a unitary PSI/PSII ratio and suboptimal ATP/NADPH ratio (Fig. 1*J*). The latter observation is consistent with the high energetic cost of PHOTOR (two ATP and one NADPH are necessary for the production of one glyceraldehyde 3-phosphate molecule from two 2-phosphoglycolate molecules) (23) and strongly suggests that PHOTOR uses a photoenergy-dissipation mechanism without extra ATP production. This suggestion is particularly interesting because excessive ATP levels is a major problem in phototrophs, leading to metabolic congestion (4). The environmental conditions in which PHOTOR is activated (18, 22), together with our in silico results, suggest a primarily role for PHOTOR as an ATP-consuming pathway under CLS. Nonetheless, an involvement in ATP-consuming futile cycles (*SI Appendix*, Fig. S10) and/or other regulatory mechanisms cannot be discounted (4).

Integrative Analysis of Photosynthesis Performance. To better understand how AEF and metabolic pathways collaborate in response to environmental perturbations, we evaluated results from our in silico analysis against published experimental observations. In particular, we investigated the reported close collaboration between the MEHLER and PHOTOR pathways in response to high-light conditions (22). In silico growth rates were first computed while having an unconstrained flux through the PHOTOR pathways and bounding the maximal possible flux through MEHLER and CYO pathways based on experimental values (Fig. 3) (27). Subsequently, we deleted either the PHOTOR or MEHLER pathways and observed significantly decreased maximal possible growth rates under CLS. The double knockout of these two pathways reduced the in silico growth rate even further (Fig. 3), which is in good agreement with experimental reports (22). These results illustrate that both pathways were required for optimal growth rates under CLS.

We then studied the collaboration between MEHLER and PHOTOR at a mechanistic level. By using the above constraints, the fluxes across the main photosynthetic reactions and the ATP/NADPH ratio were computed as a function of light availability (Fig. 3). As expected, the high photosynthetic-yield pathway CYO was the AEF pathway used by the model under LLS for ATP/NADPH balancing. The attainment of maximum flux through CYO triggered the activation of the MEHLER pathway as a new LEF-assisting pathway, leading to new suboptimal LLS. The growth rate and ATP/NADPH ratio were lower in this state because of the low photosynthetic yield of the MEHLER

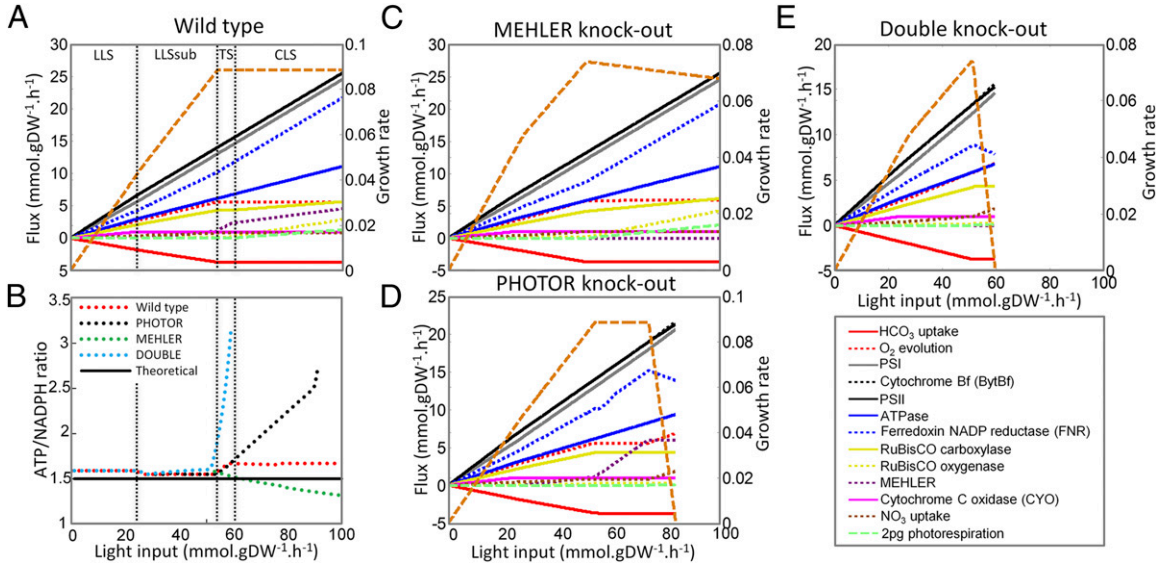

Fig. 3. Cooperativity between the MEHLER and PHOTOR pathways under high-light conditions. (*A*) The wild-type strain was simulated by constraining all fluxes in the AEF pathways to 0 mmol·gDW^{-1}·h^{-1}, except the CYO and MEHLER reactions, which were constrained to an upper bound of 1 and 6 mmol·gDW^{-1}·h^{-1}, respectively, corresponding to 6% and 40% of the electrons from PSII at the end of CLS (27). PHOTOR remained unconstrained. (*B*) ATP/NADPH ratio as a function of the light input (*SI Appendix* and Dataset S6). The theoretical optimum ratio for CO_2 fixation is indicated by a solid black line. (*C*) The MEHLER knockout was simulated by constraining the flux to 0 mmol·gDW^{-1}·h^{-1}. (*D*) PHOTOR knockout was simulated by constraining the photorespiratory metabolism (*SI Appendix*). (*E*) In the double knockout, the MEHLER and PHOTOR mutant constraints were applied. The growth rate (orange, right *y* axis) was computed under autotrophic conditions as a function of the light availability by varying the photon uptake rate from 0 to 100 mmol·gDW^{-1}·h^{-1} (*x* axis). The computed reaction fluxes are shown (left *y* axis). The functional states are denoted by LLS, LLSsub (suboptimal LLS), TS (transition state), and CLS. The boundaries between the different functional states are indicated by dotted, vertical black lines.

pathway (Fig. 3*A*). These observations indicate that low-yield pathways cannot replace the role of high-yield pathways under LLS. Before CLS, we identified a transition state in which the flux across the MEHLER reaction increased significantly. Under CLS, the flux across the MEHLER pathway increased in response to light availability, and PHOTOR was activated as an additional assistant pathway. We found that PHOTOR dissipated excess ATP to maintain ATP/NADPH balance in the wild type because no ATP dissipation was observed in PHOTOR-deficient and double-mutant strains (Fig. 3).

Our in silico analysis demonstrated the needed balancing act between MEHLER (primarily responsible for NADPH dissipation) and PHOTOR (involved in reestablishing optimal ATP/NADPH ratio via ATP dissipation) to preserve photosynthetic optimality under *Ci* depletion and/or high-light conditions.

Insights into the Heterotrophic Metabolism of *Synechocystis*. We evaluated the growth capabilities of *i*JN678 under mixotrophic and heterotrophic conditions with all of the carbon and nitrogen sources for which transport reactions were present. The model predicted growth on 10 organic carbon sources under heterotrophic conditions (*SI Appendix*, Table S4). The amino acids alanine, glutamine, and serine sustained growth in silico only under mixotrophic conditions. We characterized metabolic precursors present in *i*JN678 and identified 31 additional candidate carbon sources that could support growth in silico when specific transporters were included (in silico metabolic engineering) (*SI Appendix*, Table S5). Therefore, *i*JN678 exhibited low metabolic versatility compared with other heterotrophic bacteria, such as *Escherichia coli* (28). This analysis also suggests the presence of potential latent heterotrophic pathways encoded in the genome that could be exploited in future biotechnology applications.

*i*JN678 was used to elucidate unknown aspects of the heterotrophic metabolism in *Synechocystis*, such as the missing pyruvate oxidation pathway caused by the lack of a 2-oxoglutarate dehydrogenase (AKGDH). Computed fluxes under heterotrophic conditions indicate that glucose was metabolized to pyruvate through the oxidative branch of the pentose phosphate pathway, which agreed with experimental observations (20) (*SI Appendix*, Fig. S5). We found that pyruvate was subsequently oxidized by the combined action of the GABA shunt and the SDH complex (Fig. 4 and *SI Appendix*, Fig. S5). The contribution of SDH under heterotrophic conditions was highlighted by performing an in silico deletion of SDH that led to a reduced growth rate in the dark, but no effect on the growth rate was predicted under either mixotrophic or autotrophic conditions (Fig. 4). In

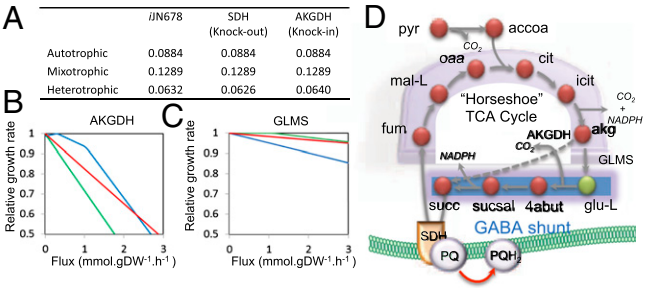

Fig. 4. Analysis of the heterotrophic metabolism in *Synechocystis*. (*A*) Effect on the growth rate (h^{-1}) of SDH knockout and AKGDH knockin. (*B* and *C*). Relative growth rate as a function of the flux through AKGDH (*B*) and GLMS (*C*) reactions on autotrophic (green), mixotrophic (red), and heterotrophic (blue) metabolisms. Optimal light conditions (photon uptake of 54.5 mmol·gDW^{-1}·h^{-1}) were used for both the mixotrophic and autotrophic metabolism. HCO_3^- (3.7 mmol·gDW^{-1}·h^{-1}) and glucose (0.85 mmol·gDW^{-1}·h^{-1}) were used as carbon sources to simulate autotrophic and heterotrophic conditions, respectively. Glucose (0.38 mmol·gDW^{-1}·h^{-1}) and HCO_3^- (3.7 mmol·gDW^{-1}·h^{-1}) were used as carbon sources under mixotrophic conditions. (*D*) Proposed complete oxidation pathway of pyruvate in *Synechocystis* under heterotrophic conditions, which involves an incomplete TCA cycle, a GABA shunt, and SDH complex. Glutamate as a common metabolite of the nitrogen assimilation pathway and the GABA shunt is indicated in green. The nonnative AKGDH reaction is indicated by a dashed arrow. See Dataset S1 for abbreviations.

the line with our results, SDH has been suggested to be the main reaction respiratory pathway providing electrons to the PQ pool in darkness but not under light conditions, where PSII plays this role (Fig. 2) (19).

We then investigated the role of the GABA shunt on heterotrophic metabolism and whether its presence is advantageous over having a complete tricarboxylic acid (TCA) cycle, which is incomplete in *Synechocystis*. We found that the inclusion of the AKGDH complex in the model, which completes the TCA cycle, increased the growth rate under heterotrophic conditions, whereas it negatively influenced the mixotrophic and autotrophic metabolism, with a stronger effect on the latter (Fig. 4 *A* and *B*). The funneling of 2-oxoglutarate (akg) to the GABA shunt through glutamate synthase (GLMS) showed the opposite effect (Fig. 4*C*). Thus, having a GABA shunt instead of a complete TCA cycle via AKGDH inclusion may represent an evolutionary advantage for *Synechocystis* in autotrophic conditions at the expense of reduced growth performance in heterotrophic conditions. Genome analysis of other cyanobacteria strengthens this hypothesis because the lack of AKGDH was preserved in this phylogenetic group, whereas the GABA shunt was found in several species (Dataset S4).

***Synechocystis* Metabolism Exhibits Low Metabolic Robustness Under Genetic Perturbations.** No experimental studies addressing essential genes and metabolic robustness from phototrophs are available. We carried out a gene essentiality and synthetic lethality analysis (Dataset S5). The highest number of essential metabolic genes was predicted under autotrophic conditions (350) followed by heterotrophic and mixotrophic conditions with 261 and 259 essential genes, respectively (*SI Appendix*, Fig. S9). Thus, a core set of 259 genes, i.e., 38% of the included genes, was found to be essential under all tested conditions, which is consistent with the 34% of essential genes reported in a previous in silico study (8). We compared our results with the mutants available in CyanoMutants (http://genome.kazusa.or.jp/cyanobase/mutants). Despite the fact that only a low number of genes could be compared, our analysis ($P < 10^{-3}$, Fisher's exact test), showed an accuracy of 79%, although a significant false positive rate (21%) was found (*SI Appendix*, Fig. S9 and Dataset S5). Many of these false positives participate in the unique pathways modeled in *i*JN678, such as photosynthetic pigments and lipid biosynthetic pathways. For instance, the genes *slr0089* and *slr1508* which are involved in the biosynthesis of tocopherols and digalactolipids, respectively, were predicted to be essential based on the presence of these metabolites in the biomass objective functions. Interestingly, in vivo data indicate that, although dispensable for growth, these metabolites are essential for acclimation to changing light conditions (29, 30). These results strongly suggest that *Synechocystis* devote many resources to preserve an optimal photosynthetic process under changing environmental perturbations, thus increasing their photosynthetic robustness.

Synthetic gene lethality is often used as a measure of metabolic robustness because synthetic essential gene products are interchangeable (isoenzymes) or operate in two separate pathways with redundant and/or complementary essential functions. This synthetic lethality analysis predicted the highest number of lethal gene deletions under mixotrophic conditions with 274, which was expected because heterotrophic and autotrophic conditions concur in mixotrophic metabolism. Conversely, the heterotrophic and autotrophic metabolic network exhibited only 234 and 158 synthetic lethal genes, respectively.

Overall, our gene essentiality and synthetic lethality analyses indicate that autotrophic metabolism requires higher numbers of genes than heterotrophic or mixotrophic metabolisms do. Therefore, the high number of metabolic essential genes in all computed growth conditions (38%) compared with other bacteria, such as *E. coli* (14.5%) (28), strongly suggests a reduced metabolic robustness in *Synechocystis*, especially in autotrophic conditions. This reduced metabolic robustness under genetic perturbation contrasts with the high photosynthetic robustness predicted (including multiple lipids, photosynthetic pigments, AEF, and metabolic pathways involved in optimal photosynthetic process). Interestingly, it has been suggested that highly evolved and specialized systems acquire high robustness against regular perturbations that but they are extremely fragile against rare perturbations (31). For *Synechocystis*, a highly specialized autotroph organism, *Ci* and/or light availability could be considered as a regular perturbation. In contrast, genetic perturbations resulting in lethal phenotypes would be rare perturbations, which only affect individual cells. Thus, the tradeoff between high photosynthetic robustness and the overall low metabolic robustness suggested by our analysis could be a consequence of the highly specialized autotrophic metabolism.

Discussion

The bottom-up metabolic network reconstruction, *i*JN678 (Dataset S7), presented here summarizes the current knowledge about the metabolism of *Synechocystis*. We investigated the optimality of photoautotrophic metabolism under both environmental and genetic perturbations and gained insight on *Synechocystis*' metabolism, including (*i*) the identification of two main states of the photosynthetic apparatus (CLS and LLS); (*ii*) the categorizing of nine AEF pathways present in *Synechocystis*; (*iii*) the high degree of cooperativity between AEF pathways required for optimizing the autotrophic metabolism; (*iv*) the critical role of PHOTOR in high-light acclimation; and (*v*) the inherently reduced metabolic versatility and robustness together with the high photosynthetic robustness derived from the photoautotrophic metabolism-specialization process.

By studying the impact of *Ci* and light availability, we have proved that multiple AEF pathways assist LEF in optimal photosynthesis performance. While under LLS, the AEF pathways provided extra ATP levels; under CLS, they dissipated the photoenergy excess (Figs. 1 and 2). The analysis of the photosynthetic and bioenergetics parameters found in *i*JN678 allowed us to classify these AEF pathways into different functional categories and may thus contribute to a better understanding of the photosynthetic process (Fig. 2). For instance, the CYO pathway had the highest Φ_{CO_2}, suggesting that this pathway is the best candidate for ATP/NADPH optimization under suboptimal light availability. Interestingly, recent studies support this nonintuitive finding, and high respiration rates together with low PSI/PSII ratios have been reported in response to low-light conditions in the deep-sea green algae *Ostreococcus* RCC809 (32). Furthermore, we showed that additional high photosynthetic-yield CEF pathways were necessary to ensure maximum growth under LLS (Fig. 3). This result is consistent with the PSI/PSII ratios greater than 1 that have been reported in phototrophs as well as with the proposed role of the NDH-1 pathway as being the main CEF pathway under suboptimal light availability (5, 14). We propose that a strong cooperativity between high photosynthetic-yield pathways assisting the LEF around PSI and PSII is required to sustain maximum growth under suboptimal light conditions. Under light excess and/or *Ci*-limited conditions, light optimization was no longer a priority but instead became a problem. These conditions led to an overreduced state, preventing growth in the absence of AEF (Fig. 1). We found that all AEF pathways identified in this study dissipated excess energy by increasing their fluxes, resulting in high ATP levels (Fig. 1). A high ATP/ADP ratio leads to acid photodamage of PSII, and several mechanisms have been proposed for ATP dissipation, including down-regulation of ATPase, controlled proton leak, metabolic futile cycles, and ATP hydrolyzing enzymes (4). Our results strongly suggest an advantage in energy dissipation of low, rather than high, photosynthetic-yield pathways for minimization of the increased ATP levels (Fig. 1*J*). Consistently, CytBD (15), FQR (14), MEHLER (16, 22), and H2ase pathways (17) are only involved in energy dissipation under high-light or *Ci*-depleted conditions (CLS). Our analysis also identified that an optimal response to CLS required the additional participation of PHOTOR as a counterpart to low photosynthetic-yield AEF pathways,

leading to energy dissipation by consuming the high ATP levels generated by these pathways (Fig. 3).

Although some microphototrophs, including *Synechocystis*, can grow heterotrophically, most of them are obligate photoautotrophs. Lesions in the central metabolism, such as an incomplete TCA cycle or the lack of organic carbon uptake systems, have been proposed as the primary causes of this obligate autotrophy (33). Thus, interesting questions arise as to why and how microphototrophs have maintained an incomplete TCA cycle and a reduced metabolic versatility even when being obligate autotrophs. We computationally showed here that the presence of the AKGDH, which may present an evolutionary advantage under heterotrophic conditions, hampered the photoautotrophic metabolism (Fig. 4). In addition, we showed that the heterotrophic metabolism of *Synechocystis* could be enhanced by the inclusion of nonnative transporters (*SI Appendix*, Table S5), suggesting missing evolutionary pressure to acquire or maintain organic carbon uptake systems. Interestingly, both the presence of the AKGDH and the inclusion of nonnative transporters have been suggested as negatively impacting the autotrophic metabolism (33–35). Our results suggest that *Synechocystis* is a highly specialized phototroph that has preserved and enhanced the photoautotrophic metabolism mainly by retaining or acquiring genes involved in controlling the light and *Ci* availability. In contrast, genes involved in the metabolism of organic carbon sources and/or potentially deleterious for autotrophic metabolism either have not been acquired or have been lost, contributing to low metabolic versatility and robustness. Thus, phototroph organisms are likely to require not only a high photosynthetic robustness but also an overall reduced metabolic robustness, avoiding reactions and pathways potentially deleterious for optimal autotrophic metabolism. The tradeoff between high photosynthetic robustness and low metabolic robustness suggested here must therefore be taken into account when designing efficient light-driven metabolic engineering processes.

Materials and Methods

A detailed description of methods, model setup, and in silico constraints used in this study can be found in *SI Appendix*. Briefly, the *Synechocystis* reconstruction was created according to published procedures (13, 36). Flux balance analysis (FBA) (37, 38) was used for model analysis. Essential and synthetic lethal essentiality analyses were performed according to the procedures described elsewhere (39). All computational simulations were performed with the COBRA toolbox (40) in the MATLAB environment (The MathWorks Inc.). The GNU Linear Programming Kit (GLPK) (http://www.gnu.org/software/glpk) was used to solve linear optimization problems.

ACKNOWLEDGMENTS. We thank Ronan M. T. Fleming for valuable discussions, Marc Abrams for critical reading of the paper, and Almut Heinken for help in compiling the SBML file. This work was supported by the US Department of Energy, Offices of Advanced Scientific Computing Research and Biological and Environmental Research as part of the Scientific Discovery Through Advanced Computing program Grant DE-SC0002009. J.N. was funded, in part, by the Spanish Ministry of Education through the National Plan for Scientific Research, Development, and Technological Innovation 2008–2011.

1. Liu X, Sheng J, Curtiss R, 3rd (2011) Fatty acid production in genetically modified cyanobacteria. *Proc Natl Acad Sci USA* 108:6899–6904.
2. Schmidt BJ, Lin-Schmidt X, Chamberlin A, Salehi-Ashtiani K, Papin JA (2010) Metabolic systems analysis to advance algal biotechnology. *Biotechnol J* 5:660–670.
3. Blankenship RE, et al. (2011) Comparing photosynthetic and photovoltaic efficiencies and recognizing the potential for improvement. *Science* 332:805–809.
4. Kramer DM, Evans JR (2011) The importance of energy balance in improving photosynthetic productivity. *Plant Physiol* 155:70–78.
5. Allen JF (2003) Cyclic, pseudocyclic and noncyclic photophosphorylation: New links in the chain. *Trends Plant Sci* 8:15–19.
6. Peltier G, Tolleter D, Billon E, Cournac L (2010) Auxiliary electron transport pathways in chloroplasts of microalgae. *Photosynth Res* 106:19–31.
7. Oberhardt MA, Palsson BO, Papin JA (2009) Applications of genome-scale metabolic reconstructions. *Mol Syst Biol* 5:320.
8. Montagud A, Navarro E, Fernández de Córdoba P, Urchueguía JF, Patil KR (2010) Reconstruction and analysis of genome-scale metabolic model of a photosynthetic bacterium. *BMC Syst Biol* 4:156.
9. Knoop H, Zilliges Y, Lockau W, Steuer R (2010) The metabolic network of *Synechocystis sp.* PCC 6803: Systemic properties of autotrophic growth. *Plant Physiol* 154:410–422.
10. Montagud A, et al. (2011) Flux coupling and transcriptional regulation within the metabolic network of the photosynthetic bacterium *Synechocystis sp.* PCC6803. *Biotechnol J* 6:330–342.
11. Fu P (2009) Genome-scale modeling of *Synechocystis sp.* PCC6803 and prediction of pathway insertion. *J Chem Technol Biotechnol* 84:473–483.
12. Shastri AA, Morgan JA (2005) Flux balance analysis of photoautotrophic metabolism. *Biotechnol Prog* 21:1617–1626.
13. Thiele I, Palsson BO (2010) A protocol for generating a high-quality genome-scale metabolic reconstruction. *Nat Protoc* 5:93–121.
14. Ooyabu J, Ohtsuka M, Kashino Y, Koike H, Satoh K (2008) The expression pattern of NAD(P)H oxidases and the cyclic electron transport pathway around photosystem I of *Synechocystis sp.* PCC6803 depend on growth conditions. *Biosci Biotechnol Biochem* 72:3180–3188.
15. Berry S, Schneider D, Vermaas WFJ, Rögner M (2002) Electron transport routes in whole cells of *Synechocystis* sp. strain PCC 6803: The role of the cytochrome *bd*-type oxidase. *Biochemistry* 41:3422–3429.
16. Helman Y, et al. (2003) Genes encoding A-type flavoproteins are essential for photoreduction of O_2 in cyanobacteria. *Curr Biol* 13:230–235.
17. Appel J, Phunpruch S, Steinmüller K, Schulz R (2000) The bidirectional hydrogenase of *Synechocystis* sp. PCC 6803 works as an electron valve during photosynthesis. *Arch Microbiol* 173:333–338.
18. Eisenhut M, et al. (2008) The photorespiratory glycolate metabolism is essential for cyanobacteria and might have been conveyed endosymbiontically to plants. *Proc Natl Acad Sci USA* 105:17199–17204.
19. Cooley JW, Vermaas WF (2001) Succinate dehydrogenase and other respiratory pathways in thylakoid membranes of *Synechocystis sp.* strain PCC 6803: Capacity comparisons and physiological function. *J Bacteriol* 183:4251–4258.
20. Yang C, Hua Q, Shimizu K (2002) Metabolic flux analysis in *Synechocystis* using isotope distribution from ^{13}C-labeled glucose. *Metab Eng* 4:202–216.
21. Young JD, Shastri AA, Stephanopoulos G, Morgan JA (2011) Mapping photoautotrophic metabolism with isotopically nonstationary ^{13}C flux analysis. *Metab Eng* 13:656–665.
22. Hackenberg C, et al. (2009) Photorespiratory 2-phosphoglycolate metabolism and photoreduction of O_2 cooperate in high-light acclimation of *Synechocystis* sp. strain PCC 6803. *Planta* 230:625–637.
23. Noctor G, Foyer CH (1998) A re-evaluation of the ATP:NADPH budget during C_3 photosynthesis: A contribution from nitrate assimilation and its associated respiratory activity? *J Exp Bot* 49:1895–1908.
24. Skillman JB (2008) Quantum yield variation across the three pathways of photosynthesis: Not yet out of the dark. *J Exp Bot* 59:1647–1661.
25. Vermaas WF, Shen G, Styring S (1994) Electrons generated by photosystem II are utilized by an oxidase in the absence of photosystem I in the cyanobacterium *Synechocystis* sp. PCC 6803. *FEBS Lett* 337:103–108.
26. Gutthann F, Egert M, Marques A, Appel J (2007) Inhibition of respiration and nitrate assimilation enhances photohydrogen evolution under low oxygen concentrations in *Synechocystis sp.* PCC 6803. *Biochim Biophys Acta* 1767:161–169.
27. Helman Y, Barkan E, Eisenstadt D, Luz B, Kaplan A (2005) Fractionation of the three stable oxygen isotopes by oxygen-producing and oxygen-consuming reactions in photosynthetic organisms. *Plant Physiol* 138:2292–2298.
28. Feist AM, et al. (2007) A genome-scale metabolic reconstruction for *Escherichia coli* K-12 MG1655 that accounts for 1260 ORFs and thermodynamic information. *Mol Syst Biol* 3:121.
29. Mizusawa N, Sakurai I, Sato N, Wada H (2009) Lack of digalactosyldiacylglycerol increases the sensitivity of *Synechocystis* sp. PCC 6803 to high light stress. *FEBS Lett* 583:718–722.
30. Schäfer L, Vioque A, Sandmann G (2005) Functional in situ evaluation of photosynthesis-protecting carotenoids in mutants of the cyanobacterium *Synechocystis* PCC6803. *J Photochem Photobiol B* 78:195–201.
31. Kitano H (2004) Biological robustness. *Nat Rev Genet* 5:826–837.
32. Cardol P, et al. (2008) An original adaptation of photosynthesis in the marine green alga *Ostreococcus*. *Proc Natl Acad Sci USA* 105:7881–7886.
33. Wood AP, Aurikko JP, Kelly DP (2004) A challenge for 21st century molecular biology and biochemistry: What are the causes of obligate autotrophy and methanotrophy? *FEMS Microbiol Rev* 28:335–352.
34. Zhang C-C, Jeanjean R, Joset F (1998) Obligate phototrophy in cyanobacteria: More than a lack of sugar transport. *FEMS Microbiol Lett* 161:285–292.
35. Vázquez-Bermúdez MF, Herrero A, Flores E (2000) Uptake of 2-oxoglutarate in *Synechococcus* strains transformed with the *Escherichia coli kgtP* gene. *J Bacteriol* 182:211–215.
36. Thorleifsson SG, Thiele I (2011) rBioNet: A COBRA toolbox extension for reconstructing high-quality biochemical networks. *Bioinformatics* 27:2009–2010.
37. Varma A, Palsson BO (1994) Metabolic flux balancing: Basic concepts, scientific and practical use. *Nat Biotechnol* 12:994–998.
38. Orth JD, Thiele I, Palsson BO (2010) What is flux balance analysis? *Nat Biotechnol* 28:245–248.
39. Pál C, et al. (2006) Chance and necessity in the evolution of minimal metabolic networks. *Nature* 440:667–670.
40. Schellenberger J, et al. (2011) Quantitative prediction of cellular metabolism with constraint-based models: The COBRA Toolbox v2.0. *Nat Protoc* 6:1290–1307.

SI Appendix: Table of contents

List of Supplementary tables, figures and datasets

Supplementary tables

Supplementary figures

Datasets

Supplementary Information

1. Enhancements of the reconstructed *Synechocystis* network

The properties of *Synechocystis* PCC8063 genome-scale reconstruction are shown in Table S1. The major areas of enhancement over previous metabolic reconstructions of *Synechocystis* are summarized in Table S2 and are as follows:

Photosynthetic specific pathways. We modeled in detail oxidative phosphorylation and the photosynthetic apparatus of *Synechocystis* by taking into account that, while the thylakoid membrane contains both photosynthetic and respiratory electron transport chains, only the respiratory chain is present in the cytoplasmic membrane (Fig. S1) (1). The oxidative phosphorylation pathway includes NDH-1, NDH-2, NDH-1_3, and NDH-1_4 NAD(P)H dehydrogenase complexes (2), the membrane-associated succinate dehydrogenase complex SDH (1), two aa3-type terminal oxidases (CtaI and CtaII, CYO) (3), and the plastoquinone oxidase (CydBD) (3), together with ATPase complexes (4). The photosynthetic electron chain includes photosystem II (PSII), cytochrome b_6f (CYTBF), photosystem I (PSI), and the ferredoxin $NADP^+$ oxidoreductase (FNR) as components of the linear electron chain (LEF) (4). In addition, the ferredoxin plastoquinone reductase (FQR) reaction was included (5, 6). Auxiliary photosynthetic electron transport pathways, such as the MEHLER reaction (7) and the bidirectional hydrogenase (8) were also included in the reconstructed photosynthetic apparatus (Fig. S1). Based on the presence of an efficient inorganic carbon concentration mechanism in *Synechocystis* (9), it was assumed that cyanobacteria do not possess photorespiration. However, recent reports have shown that an active photorespiratory metabolism is present in *Synechocystis*, employing a plant-like glycolate cycle, a bacterial-like glycerate pathway, and complete decarboxylation of glyoxylate *via* formate (10). The three photorespiratory pathways were included in the metabolic reconstruction. Another important set of pathways, included are those involved in the synthesis of photosynthetic pigments. *i*JN678 contains complete biosynthetic pathways for chlorophyll a, lycopene, and other carotenoid compounds, including β-carotenoids, zeaxanthin, and equinone. Biosynthetic pathways for α-, β-, γ- and δ-tocopherol were also included. Beyond their role in photosynthesis (11, 12), these metabolites are of biotechnological interest as they have a high added value (13).

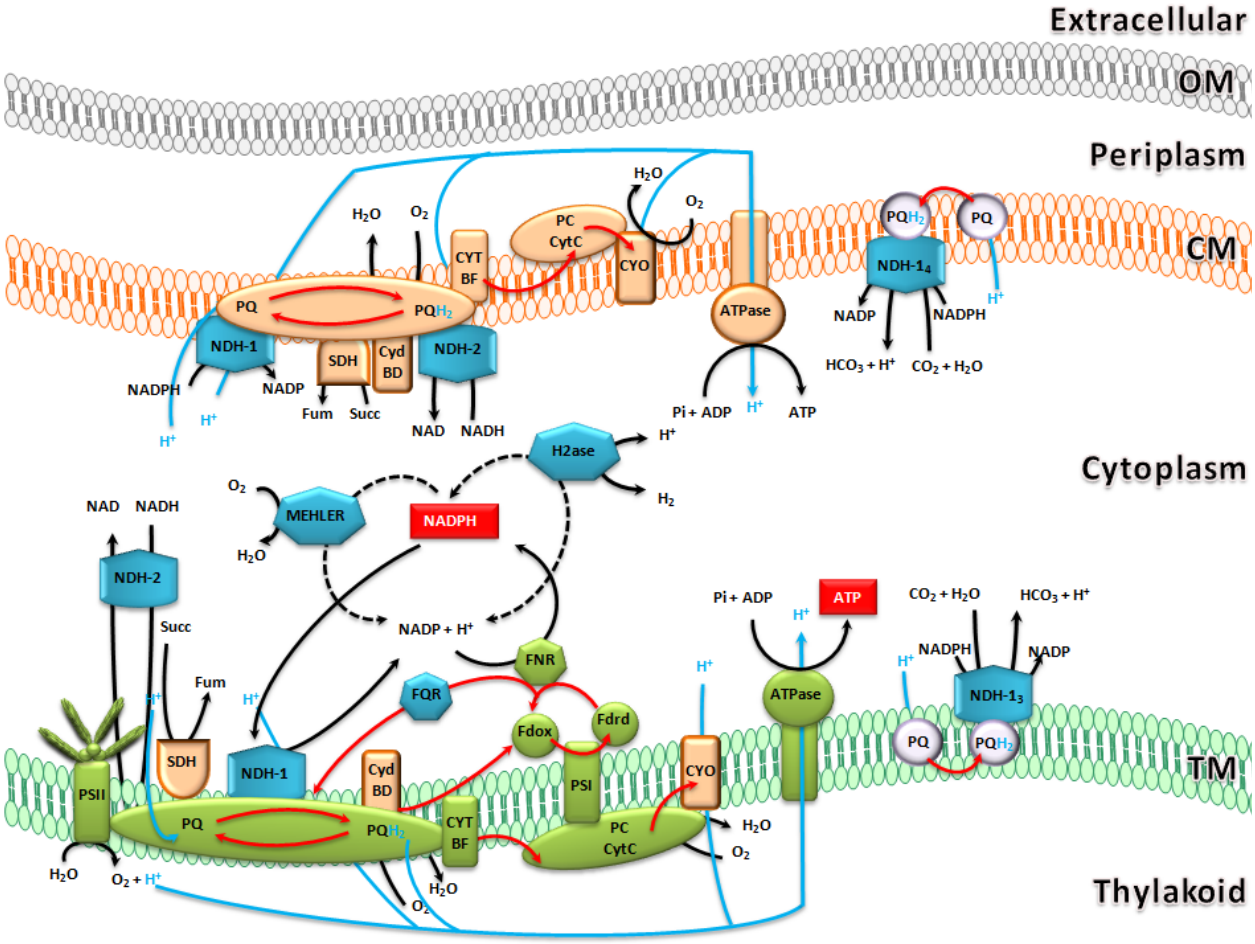

Figure S1. **Modeling of the oxidative phosphorylation and photosynthetic pathways included in *i*JN678.** The four compartments included in the reconstruction, i.e., extracellular, periplasm, cytoplasm and thylakoid separated by the outer (OM), cytoplasmatic (CM) and tylakoid (TM) membranes, are indicated. The photosynthetic linear electron flow (green) and the respiratory (orange) pathways as well as the accessory photosynthetic and respiratory branches (in blue) are placed in the right locations. The abbreviations used are: SDH, succinate dehydrogenase complex; PQ, plastoquinone; CYTBF, cytochrome $Cytb_6f$; PC, plastocyanine; CytC, cytochrome c6; CYO, cytochrome oxidase; CYTBD, plastoquinone oxidase; PSI, photosystem I; Fdox, oxidized ferredoxin; Fdrd, reduced ferredoxin; FNR, ferredoxin $NADP^+$ reductase; FQR, ferredoxin plastoquinone reductase; H2ase, bidirectional hydrogenase; MEHLER, Mehler reaction; ATPase, ATP synthetase; NDH-1, NADPH dehydrogenase complex 1; NDH-2, NADH dehydrogenase; NDH-1_3, NADPH dehydrogenase complex 3; NDH-1_4, NADPH dehydrogenase complex 4. The flux of electrons and protons through the photosynthetic and respiratory pathways is indicated by red and blue arrows, respectively. The final photosynthetic products, i.e., ATP and NADPH, are shown by red squares.

Lipids modeling. Modeling of lipids biosynthetic pathways poses a real challenge in metabolic reconstructions due to the limited amount of information available. As a consequence, the fatty acid biosynthesis is often partially modeled and only the intermediates are included in the biomass objective function (14). Given the metabolic and biotechnological importance of fatty

acid biosynthesis in *Synechocystis* (15) and the fact that a wealth of information about lipids biosynthesis is available for *Synechocystis* (16), the four classes of lipids present in *Synechocystis* were modeled in detail. Thus, biosynthesis pathways were modeled for the glycolipids monogalactosyldiacylglycerol (MGDG), digalactosyldiacylglycerol (DGDG) and sulfiquinovosyldiacylglycerol (SQDG) and the phospholipid phosphatidylglycerol (PG) (Dataset S2). Acyl-lipid desaturase reactions were included on the basis of the genetic and biochemical information available (17). The model therefore accounts for many relevant polyunsaturated lipids, e.g., ω-3 fatty acids. A detailed list of fatty acids and lipids included in the reconstruction is shown in Dataset S2.

Transport reactions. Active transport appears to be the primary means by which microorganisms acquire organic carbon and other substrates from the environment. A detailed analysis of transport systems is therefore a first step in the study of the heterotrophic metabolism of a particular organism. Transport reactions have received limited attention in previous reconstructions of *Synechocystis* despite their critical roles in cell metabolism (18-22). These reactions largely determine the metabolites that can be used in the reconstruction as biomass precursors and energy sources. A total of five different inorganic carbon uptake systems have been identified in *Synechocystis*: three HCO_3^- transporters (the BicA, SbtA and BCT systems) and two CO_2 uptake systems mediated by the NDH-1_3 and NDH-1_4 dehydrogenase complexes (9). Several transporter systems for nitrogen (23), sulfur (24), phosphate (25), metals and other anions have been identified as well. Transport systems for neutral amino acids and histidine, for basic amino acids and glutamine as well as for glutamate, have also been identified (26). All of these transporters were included in the model, together with the well-known glucose and fructose transporter GlcP (27). Furthermore, non-gene-associated transport reactions for several organic acids such as pyruvate, oxoglutarate and citrate were included on the basis of experimental evidence (19, 28-30) (Dataset S1). It is important to note that no outer-membrane transporters are encoded in the genome of *Synechocystis* (http://genome.kazusa.or.jp/cyanobase). This suggests a high permeability of the *Synechocystis* outer membrane compared to other bacteria such as *Pseudomonas,* in which numerous outer membrane porins circumvent the low permeability of their outer membranes (31). Based on this assumption, the transport through the outer membrane was modeled by using passive diffusion transport reactions (Dataset S1).

A total of 221 genes encoding 168 potential transporters have been predicted in *Synechocystis* (http://www.membranetransport.org/), implying 47.06 transporters per Mb of genome, a significantly smaller number of transporters compared with other metabolic versatile gram-negative bacteria such as *E. coli* and *P. putida* KT2440, 76.96 and 63.28 transporters per Mb respectively (http://www.membranetransport.org/). A functional classification of the genes encoding for transporters in the *Synechocystis* genome showed, as expected for a photosynthetic microorganism, that more than 50% are involved in the uptake of inorganic metabolites (Fig. S2). Interestingly, 10% of the transporters in *Synechocystis* encode for putative sugar and organic acid transporters and approximately 12% are involved in amino acid uptake systems, suggesting an important role of heterotrophic metabolism in this cyanobacterium. A comparison of the genes encoding for transporters encoded in the *Synechocystis* genome and those that were included in *i*JN678 is shown in Fig. S2.

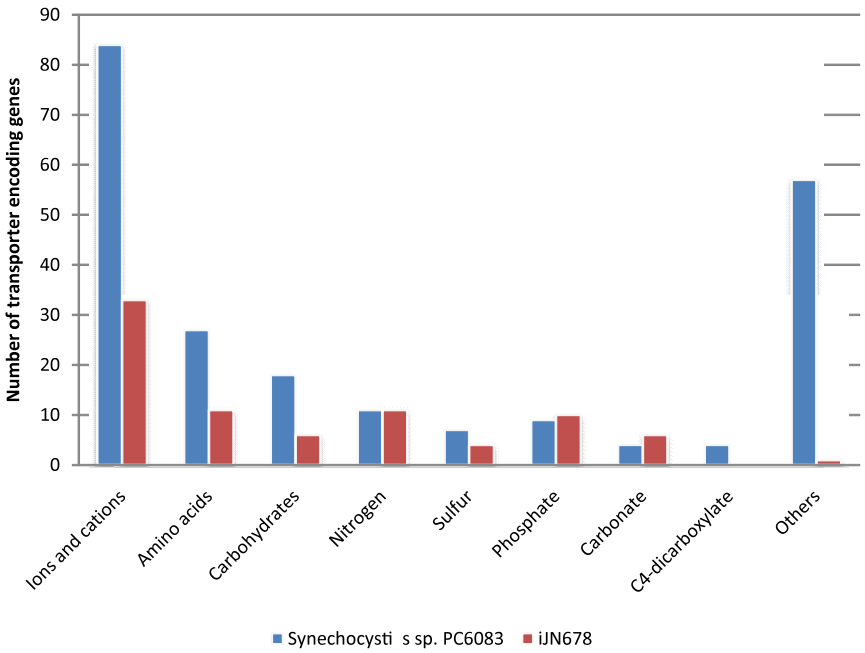

Figure S2. Transport modeling. Predicted transporter-encoding genes in *Synechocystis* (blue bars) compared with the transporter-encoding genes included in *i*JN678 (red bars).

Mass and charge balance. Environmental changes, such as variations in pH, temperature or osmolarity, can alter the trans-membrane proton motive force and consequently affect the internal homeostasis of the cell as well as the energy production. In order to maintain internal homeostasis, cells have to regulate the internal pH by secreting or consuming protons in steady-state conditions. Reactions in *i*JN678 are completely mass and charge balanced in contrast to previous metabolic reconstructions (19, 20, 22) of *Synechocystis* and account for all the protons being generated and consumed; thus, the internal and external proton balancing can be investigated *in silico* (32), see below.

Biomass reaction. The formulation of a detailed biomass objective function (BOF) in a metabolic reconstruction is critical for model evaluation and quantitative predictions and realistic gene essentiality analysis (33). The BOFs included in previous *Synechocystis* reconstructions account mainly for amino acid, fatty acid and nucleic acid precursors (18-22). The biomass presented here accounts for the major biomass constituents and their fractional contributions to the overall cellular biomass. It was derived from the literature and estimated from genomic content, Dataset S2.

A brief comparison between *i*JN678 and the available *Synechocystis* reconstructions is provided in table S2. In addition, we performed a quantitative and qualitative comparison between *i*JN678 and *i*Syn699 (22) and *i*Syn811 (21), recently published *Synechocystis* metabolic reconstructions. Since the gene content of *i*Syn811 is not publicly available, we only carried out gene content comparison between *i*JN678 and *i*Syn699 (22). We found that a total of 567 genes are included in both reconstructions, 170 genes are only included in *i*JN678 and 80 genes are only present in *i*Syn669 (Dataset S1). Genes exclusive to *i*JN678 encode mainly for reactions involved in photosynthesis, oxidative phosphorylation, photo-respiration, lipids and photosynthetic pigments biosynthesis, transport and *Synechocystis*-specific storage polymers, such as cyanophicin and poly-hydroxybutyrate (Dataset S1). On the other hand, reactions associated with genes only present in *i*Syn669 include biosynthetic pathways not included in *i*JN678 such as lipoic acid, DNA and RNA polymerization. These disparities provide an interesting target for further expansions of the current *Synechocystis* metabolic reconstructions.

On the other hand, since the number of blocked reactions in *i*Syn811 were reported (21), we also decided to identify blocked reactions in *i*JN678 in order to compare the connectivity in both models (Dataset S1). *i*Syn811 includes a higher number of reactions than *i*JN678 (956 versus 863, table S2). However, while the number of blocked reactions in *i*Syn811 ranges between 377 and 394 under auto and heterotrophic conditions, respectively only 182 and 188 blocked reaction were found in *i*JN678 under the same conditions (Dataset S1). In addition, many of blocked reactions in *i*JN678 are involved in alternative carbon and nitrogen sources, which carry flux when the appropriate carbon or nitrogen source is present in the simulation. In fact, there are only 125 blocked reactions (15.5%) in *i*JN678 when all the possible carbon and nitrogen source are included in the simulation (Table S1). This indicates that while our reconstruction has a lower number of reactions, it exhibits more connectivity and a higher number of active reactions.

Subsystems	54
Reactions	863
Metabolic reactions	706
Transport reactions	109
Orphan reactions (% of network)	127 (14%)
Exchange reactions	48
[¶]Blocked reactions (% of network)	125 (14%)
Metabolites	795
Total genes in *Synechocystis*	3725
Genes (% of genome)	678 (18%)
Number of references included	248
% reactions with reference associated	57%
[a]SKI value	0.70

Table S1. Characteristics of the reconstructed metabolic network of *Synechocystis.* [¶]Blocked reactions were computed by leaving all the exchange reactions unconstrained (lower/upper bounds of -/+ 10^3 mmol/gDW/h). [a]Species Knowledge Index (SKI) was calculated as described in (34).

Model Name	Genes	Reactions	Metabolites	[a]BOF Level	Photosynthesis Modeling	Lipid Modeling	Complete Mass /Charge Balancing	Compartments	Reference
***i*JN678**	678	863	795	Advance	Complete	Complete	Yes	[e],[p],[c],[u]	This study
-	Nd	93	Nd	Basic	Lumped	No	No	[e],[c]	(18)
-	78	56	72	Basic	Lumped	No	No	[e],[c]	(35)
-	505	652	701	Basic	Lumped	No	No	[e],[c]	(19)
-	Nd	46	29	Basic	Lumped	No	No	[e],[c]	(36)
-	343	380	291	Intermediate	Lumped	[d]Partial	No	[e],[c]	(20)
iSyn669	[b]669	882	790	Intermediate	[c]Complete	[d]Partial	No	[e],[c]	(22)
iSyn811	881	956	911	Intermediate	[c]Complete	[d]Partial	No	[e],[c]	(21)

Table S2. **Comparison of *i*JN678 with previous metabolic reconstructions from *Synechocystis*.** [a]BOF level definition was taken from (33). [b]Only 589 genes were found in the Additional File 1: 'iSyn669 reactions to gene connections" (22). [c] *i*Syn669 and *i*Syn811 lack of key photosynthetic pathways such as MEHLER and PHOTOR, well-compartmentalized photosynthetic modeling and the interaction between respiration and photosynthesis is not captured. [d] These models include fatty acid biosynthesis pathways but they lack of phospho- and photosynthetic-specific lipids modeling. Compartments symbols were taken from (14). [e] extracellular space; [p] periplasm; [c] cytoplasm; [u] thylakoid.

2. *i*JN678 represents a database of current biochemical, genetic and genomic (BiGG) knowledge about *Synechocystis*

A confidence score was assigned to each reaction in the network on the basis of available experimental evidence. *i*JN678 therefore represents a comprehensive knowledge base that summarizes and categorizes the information currently available for *Synechocystis*. On completion, the reconstruction had an overall average confidence score of 2.87. In fact, 57% of the metabolic reactions in *Synechocystis* included in *i*JN678 have been very well or well-studied, while 43% were primarily based on the genome annotation. A heat map depicting the experimental evidence available for the different subsystems is shown in Fig. S3. This categorization allowed us not only to identify well-known metabolic pathways in *Synechocystis*, but also to identify those pathways that are poorly understood. Future research efforts should be directed towards this latter group. In this sense, the current knowledge reflects the traditional use of *Synechocystis* as a photosynthetic-model bacterium and subsystems such as the photosynthetic pathways and the biosynthesis of photosynthesis pigments are well studied. In contrast, the *Synechocystis* subsystems involved in cofactor biosynthesis, such as riboflavin, vitamin B6, thiamine, pantothenate, biotin and folate, along with the subsystems involved in the synthesis of amino acids and nucleotides, are in need of further characterization (Fig. S3).

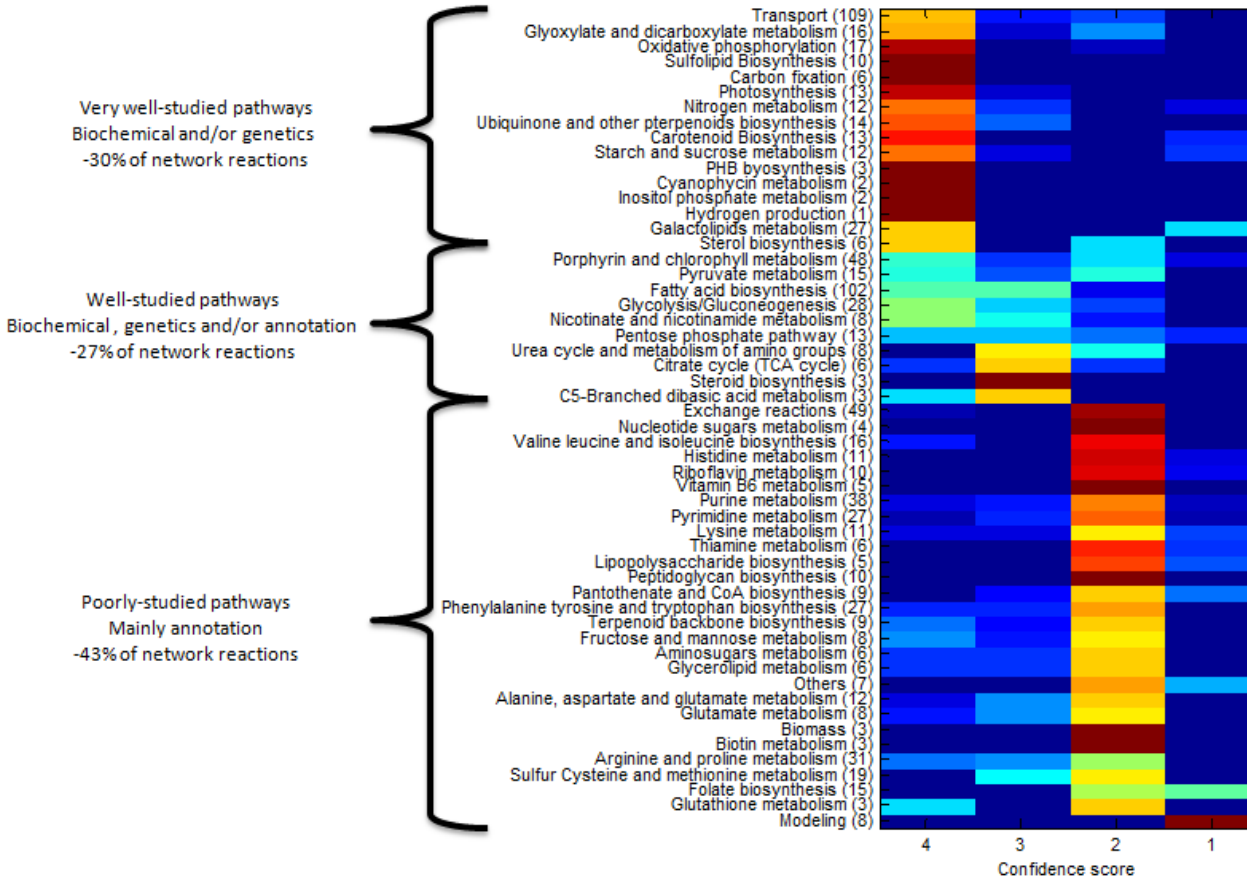

Figure S3. A comprehensive knowledge base that summarizes and categorizes the information currently available for *Synechocystis*. Subsystems and number of reactions in each subsystem are listed. The various colors correspond to the percentage of subsystems reactions that have the corresponding confidence score (red = 100%, blue = 0%). The confidence level was based on a scale from 1 to 4. A score of 4 was assigned when are available direct experimental evidence for gene product function and biochemical reaction; 3 represents physiological, genetic, or proteomic evidence; 2 corresponds to only genome annotation evidence for a gene product and its reaction(s); and finally a score of 1 reflects that no evidence is available, but the reaction is required for modeling functionality (e.g., production of biomass precursor).

3. Computation of the *Synechocystis* growth rate

Comparisons of *in silico* growth rates with experimental data are valuable in network evaluation. The growth capability of *i*JN678 in BG-11 *in silico* medium (*i*BG-11) (see Supplementary Methods) under autotrophic, mixotrophic and heterotrophic conditions was determined by using flux balance analysis (FBA) and experimentally determined carbon uptake rate as constraints (Table S3). Under heterotrophic conditions at the expense of glucose as the sole carbon and energy source, *i*JN678 exhibited a slightly lower growth rate than the experimental reported values (0.063 h^{-1} vs 0.076 h^{-1}), (37). In addition, Yang et al reported an interesting mixotrophic culture condition in which atmospheric CO_2 was removed and,

consequently, only intracellular CO_2 was available. By simulating these conditions, *i*JN678 exhibited a growth rate that was practically identical to the experimental values (Table S3). This agreement is only one example of the predictive potential of the COBRA approach and it shows how the *in silico* predictions can become precise by using additional constraints. Autotrophic conditions were simulated by constraining the CO_2 uptake rate to -3.7 $mmol.gDW^{-1}.h^{-1}$ (18) while the light uptake rate remained unconstrained. The growth rate was a function of the light and availability of CO_2 under these conditions (Fig S4). The predicted phototrophic maximal growth rate was almost identical to the experimentally reported growth rate (18, 38) (Table S3). The photosynthetic quotient defined as moles of O_2 released per mole of CO_2 fixed was estimated as 1.51. This value falls within the observed range for several photosynthetic organisms (18, 39). The minimum photon uptake rate necessary for maximal growth was calculated to be 54.5 $mmol.gDW^{-1}.h^{-1}$. Taking the typical mass and diameter of a *Synechocystis* cell, 0.5 pg and 1.75 μm respectively (18), and assuming the maximal efficiency of photosynthesis to be 4.6 - 6% (40), the optimal photon uptake translates to a irradiance of approximately 13.14 - 17.14 $\mu E.m^2.s^{-1}$ which is close to the minimum light intensity required for optimal growth of *Synechocystis* and other cyanobacteria, 15 - 75 $\mu E.m^2.s^{-1}$ (41).

Culture		***Growth rate*** **μ (h^{-1})**	***Glucose uptake*** **q_{glc} ($mmol/g_{DW}/h$)**	***O_2 evolution*** **q_{O2} ($mmol/g_{DW}/h$)**	***CO_2 evolution*** **q_{CO2} ($mmol/g_{DW}/h$)**
Heterotrophic	*Synechocystis* [37]	0.076	0.85	Nd	1.99
	*i*JN678	0.063	<u>0.85</u>	(-)1.18	2.53
Mixotrophic	*Synechocystis* [37]	0.059	0.38	Nd	0.0
	*i*JN678	0.056	<u>0.38</u>	1.19	[a]<u>0.0</u>
Autotrophic	*Synechocystis*[18]	0.085	0.0	4.82	(-) 3.7
	*i*JN678	0.088	<u>0.0</u>	5.58	(-) <u>3.7</u>

Table S3. **Comparison of growth rates of the *in silico* strain *i*JN678 and *Synechocystis.*** Environmental constraints applied in the simulations are underlined. [a]*Ci* uptake was not allowed according to the mixotrophic conditions reported by Yang et al (37).

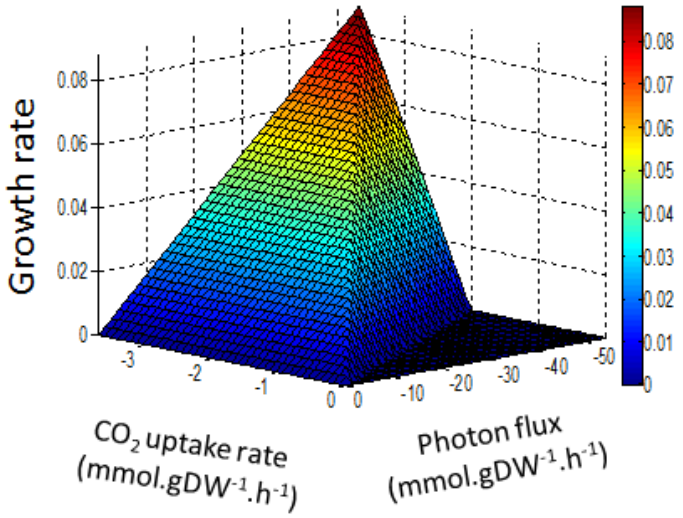

Figure S4. *Synechocystis*'growth under autotrophic conditions as a function of photon and CO_2 uptake.

4. Internal flux distributions: prediction and validation

Metabolic flux analysis (MFA) is a powerful tool for understanding CO_2 fixation and light-energy utilization of photosynthetic organisms during photoautotrophic cultivation. However, techniques for experimental measurement of system-wide metabolic fluxes in purely photoautotrophic systems (using CO_2 as the sole carbon source) have not yet been well developed and metabolic flux quantification in photosynthetic organisms is difficult to perform on a systemic level. Consequently, the metabolic flux distribution in photosynthetic organisms remains poorly understood (42). The *in silico* flux distributions corresponding to maximum growth were obtained by maximizing the biomass objective function. Comparisons with experimental flux values are not only a useful tool for validating the model but also for the generation of new hypotheses.

In heterotrophic growth conditions, glucose was funneled mainly through the oxidative pentose phosphate (OPP) pathway, followed by the NAD-dependent glyceraldehyde-3-phosphate dehydrogenase (GAP1), which drives the carbon flux to the incomplete TCA cycle (Fig. S5, Dataset S3). Our results were in good agreement with previous experimental data (37, 43, 44) (τ = 0.89), and computational predictions (18, 20, 35). The high flux through the OPP, glucose 6-phosphate dehydrogenase (G6PDH) and phosphogluconate dehydrogenase (GND) and the flux across GAP1, as well as the significant flux across the TCA cycle (mainly the NADPH-dependent isocitrate dehydrogenase) provides reducing power in the form of NAD(P)H. In

addition, the TCA cycle supplied important biosynthetic precursors together with carbon skeletons for nitrogen fixation in the form of 2-oxoglutarate (Fig. S5). Interestingly, our *in silico* analysis suggested that succinate was generated through the GABA shunt (Fig. S5), while the succinate semialdehyde dehydrogenase (SSALyr) further increased the NADPH levels. Finally, the reducing power was oxidized by the NADPH and SDH dehydrogenase complexes, contributing to energy production under heterotrophic conditions which supports previous reports (1, 30) (Fig. S5).

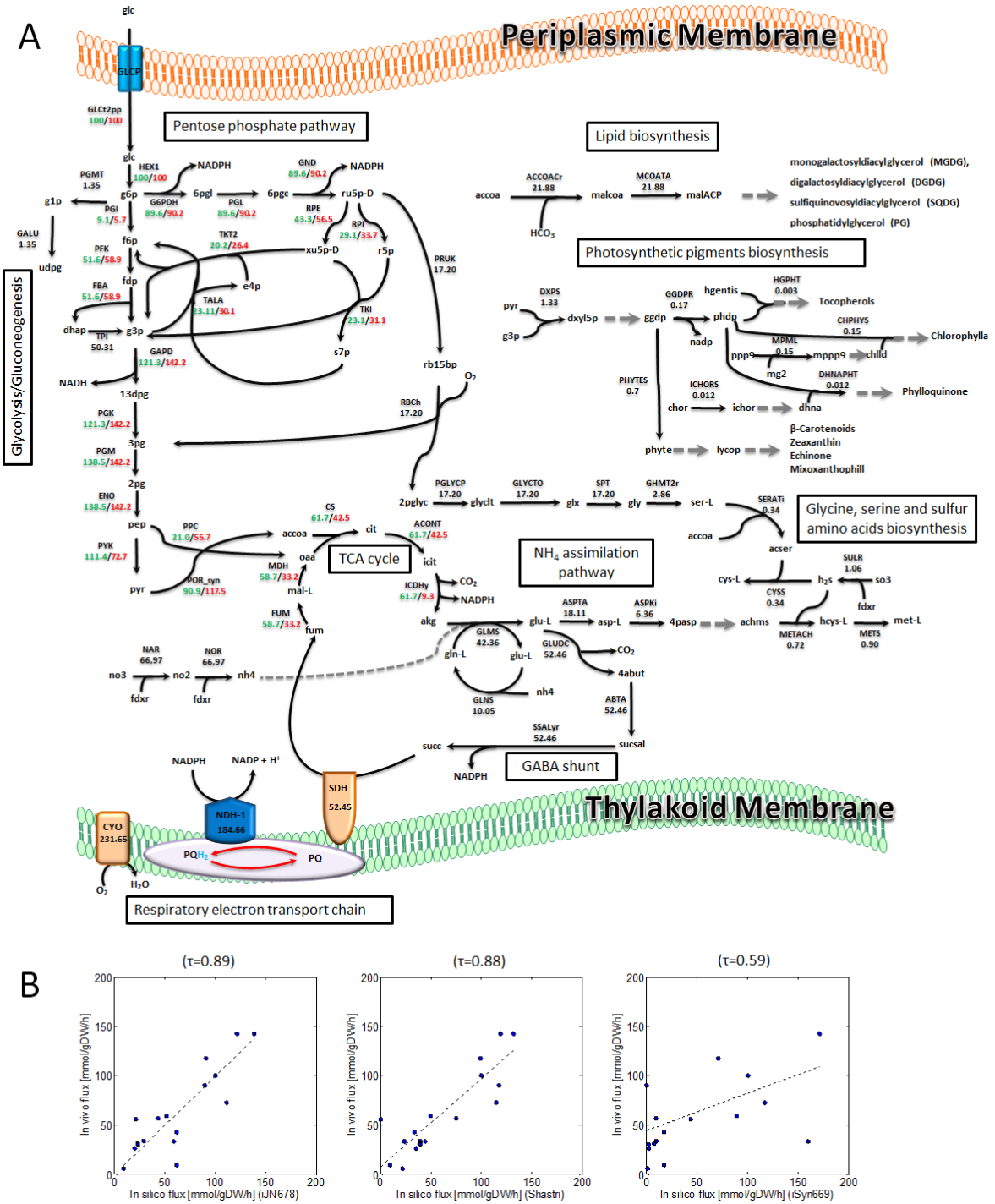

Figure S5. Flux distribution predicted under heterotrophic conditions. **(A)** Predicted flux values (green) compared with the experimental flux values (red) reported by Yang et al (37) under heterotrophic conditions. Values in black represent *in silico* flux predictions for which no experimental data are available. The net fluxes were normalized to the glucose uptake rate, which was 0.85 mmol/gDW/h. Metabolic pathways involved in the central, nitrogen, and sulfur metabolisms as well as those modeled for first time in *i*JN678 are shown in black boxes.. Arrows indicate the direction of the estimated fluxes. The flux distribution was obtained by FBA. **(B)** *In vivo* and *in silico* flux values correlation expressed as Kendall's rank correlation coefficient (τ) for *i*JN678, the central metabolism reconstruction from Shastri and Morgan (18) and *i*Syn699 (22).

Under autotrophic conditions, the photosynthetic apparatus generates the reducing power and produces ATP. The flux map obtained under these conditions therefore reveals a completely different carbon-flux distribution compared to heterotrophic conditions (Fig. S6, Dataset S3). The RuBisCO provided 3-phosphoglycerate (3PG), which was split towards the TCA cycle, led by the phosphoglycerate mutase (PGM) and the Calvin cycle, and driven by the phosphoglycerate kinase (PGK). The PGM / PGK ratio of 1/7.6 is slightly higher than the textbook ratio of 1/5 due to the demand of precursors for biosynthesis but is close to previous computational estimations (18, 20). In contrast to the heterotrophic flux distribution, we found that the production of pyruvate under autotrophic conditions relied mostly on the $NADP^+$-dependent malic enzyme (ME1) and not from pyruvate kinase (PYK) (Fig. S5-6). This data, although in contrast with the previous computational flux predictions (18), has been recently validated by in vivo flux distribution data (45), and is in good agreement with an experimental study where the pyruvate pathway was found to involve phosphoenolpyruvate carboxylase (PPC), malate dehydrogenase (MDH) and ME1 (29). The calculated flux distribution was also consistent i) with the observation that *cyanobacteria* can convert significant amounts of CO_2 into malate in light conditions (46) and ii) with the properties of a C_4-like photosynthetic metabolism through phosphoenolpyruvate synthase (PPS) and ME1, which has been described for *cyanobacteria* (37).

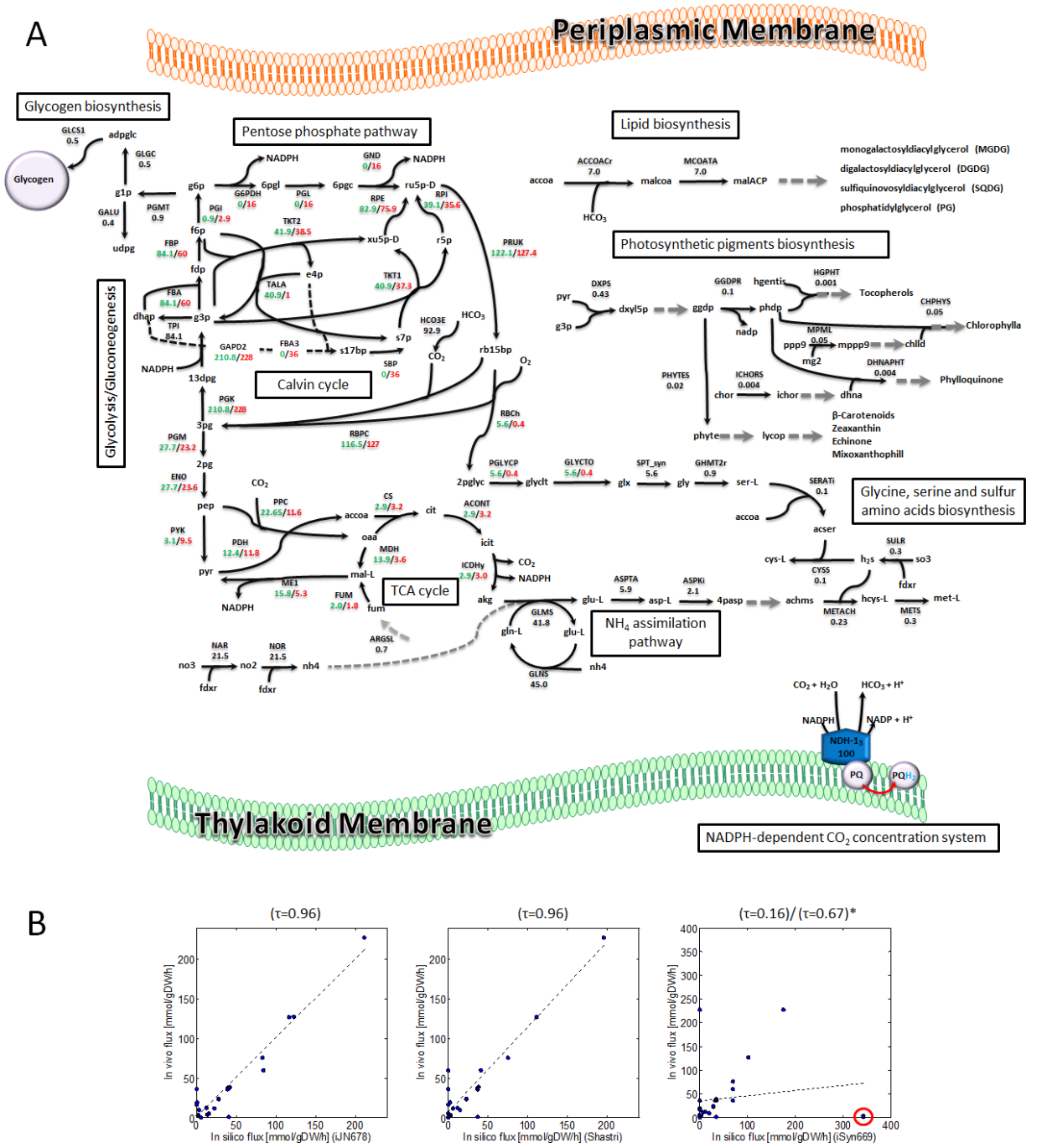

Figure S6. Flux distribution predicted under autotrophic conditions. **(A)** Predicted flux values (green) compared with the previous flux values predictions (red) reported under autotrophic conditions (45). Values in black represent *in silico* flux predictions for those reactions for which no experimental data have been reported. The net fluxes were normalized to the CO_2 uptake rate, which was 3.7 mmol/gDW/h. Metabolic pathways involved in the central, nitrogen, and sulfur metabolisms as well as those modeled for first time in *i*JN678 are shown in black boxes. Arrows indicate the direction of the estimated fluxes. The flux distribution was obtained by FBA. **(B)** *In vivo* and *in silico* flux values correlation expressed as Kendall's rank correlation coefficient (τ) for *i*JN678, central metabolism reconstruction from Shastri and Morgan (18) and *i*Syn699 (22).*(τ) value excluding malate dehydrogenase and fumarase (red circle) for *i*Syn669.

On the other hand, the oxygenic activity of the RuBisCO was found to represent 4.5% of the total RuBisCO activity, an estimated value that agrees well with early reported data (4-5%) (20). In addition, the 2-phosphoglycolate that was produced was a key intermediate in the synthesis of glycine, serine and cysteine (Fig.S6). Because no significant fluxes through the GABA shunt or SDH were predicted in our analysis, the optimal flux distribution around the TCA cycle therefore reflects an incomplete TCA cycle in which fumarate was mainly synthesized from arginine.

Under mixotrophic conditions, glucose was metabolized via the non-oxidative pentose phosphate pathway to produce ribulose-1,5-diphosphate. Furthermore, 3PG was produced by RuBisCO and followed the same flux distribution as described above for the autotrophic condition (Fig S7, Dataset S3). However, the PGM/PGK ratio was reversed under mixotrophic conditions due to the flux of exogenous glucose to fructose-6-phosphate. Pyruvate was mainly produced by PYK. Another interesting characteristic of the mixotrophic metabolism was that a small but significant respiratory rate is predicted for maximum growth under this condition. Overall, these results provide evidence, as was expected, for the concurrence of both autotrophic and heterotrophic metabolism under mixotrophic conditions (Fig. S7, Dataset S3).

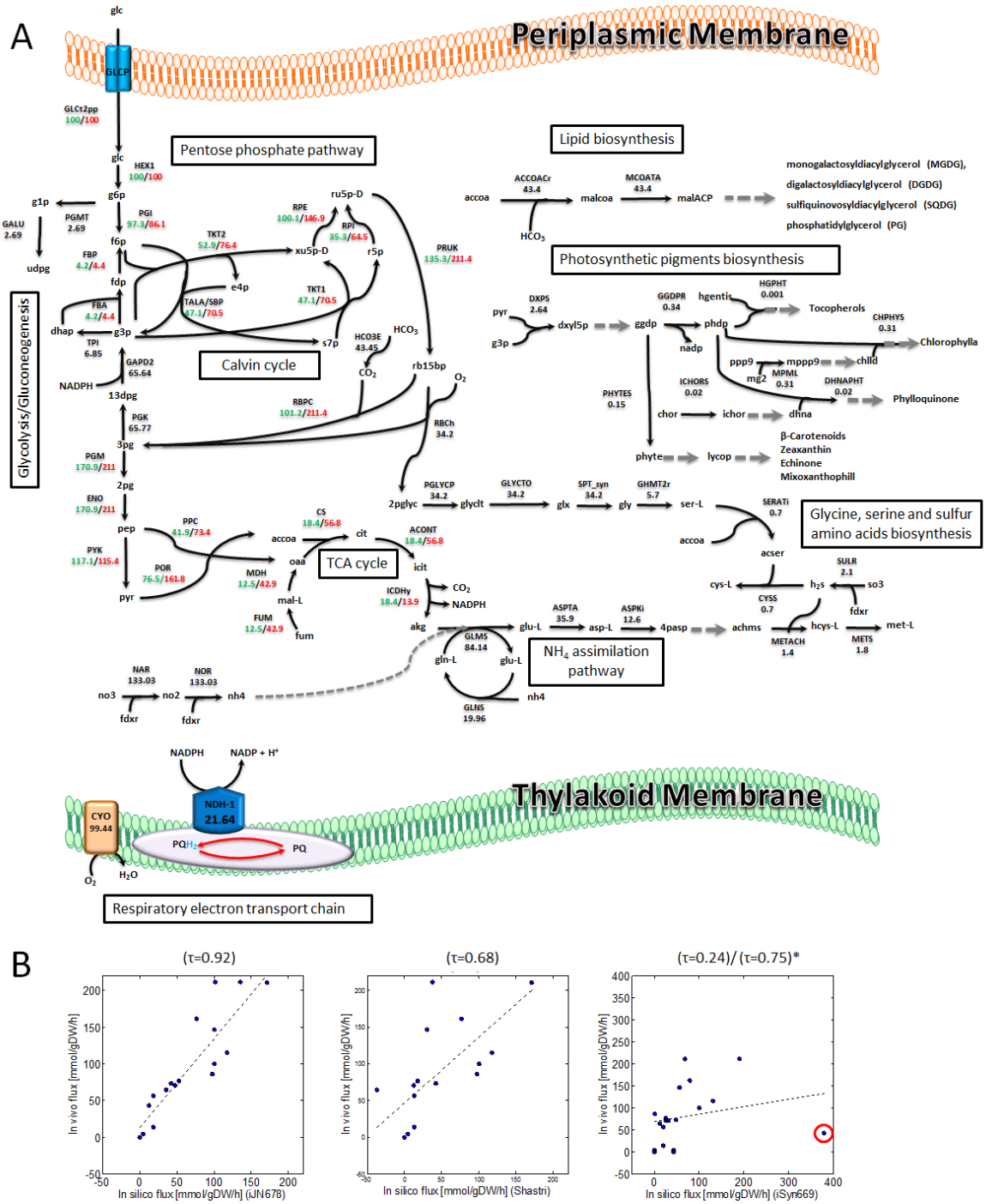

Figure S7. Flux distribution predicted under mixotrophic conditions. (A) Predicted flux values (green) compared with the experimental flux values (red) reported by Yang et al (37) under mixotrophic conditions. Values in black represent *in silico* flux predictions for those reactions for which no experimental data have been reported. The net fluxes were normalized to the glucose uptake rate, which was 0.38 mmol/gDW/h, no CO_2 uptake was allowed in the simulation following the culture conditions used by Yang et al. Metabolic pathways involved in the central, nitrogen, and sulfur metabolisms as well as those modeled for first time in *i*JN678 are shown in black boxes. Arrows indicate the direction of the estimated fluxes. The flux distribution was obtained by FBA. **(B)** *In vivo* and *in silico* flux values correlation expressed as Kendall's rank correlation coefficient (τ) for *i*JN678, central metabolism reconstruction from Shastri (18) and *i*Syn699 (22).* (τ) value excluding malate dehydrogenase and fumarase (red circle) for *i*Syn669.

The correlation between the *in vivo* flux distribution data and those estimated *in silico* with *i*JN678, *i*Syn669 and the central metabolism reconstruction from Shastri and Morgan was estimated using Kendall's rank correlation coefficient in order to estimate the accuracy of our flux distribution predictions. *i*Syn669 was selected because it was used in an exhaustive flux distribution analysis under various culture conditions (22). The reconstruction of Shastri and Morgan was selected because it was the first metabolic reconstruction published and because this model has been used for computing *in vivo* flux distribution data under autotrophic conditions (45). We found that the flux distribution estimated with *i*JN678 correlated well with *in vivo* flux distributions under hetero, mixo and autotrophic conditions (τ = 0.89, 0.92 and 0.96 respectively) (Fig. S5-7). The prediction accuracy of *i*JN678 was slightly higher than for the Shastri reconstruction, but significantly higher than for *i*Syn669. *i*Syn699 was able predict flux distribution under heterotrophic conditions with moderate accuracy, but failed to predicts flux distribution under mixotrophic and autotrophic conditions. The modeling of the glucose metabolism under heterotrophic conditions has been well established and numerous metabolic reconstructions include it. The autotrophic metabolism is however, still under development. The high prediction accuracy found in *i*JN678 highlights the detailed modeling of the autotrophic metabolism found in our reconstruction and makes *i*JN678 a template reconstruction for further genome-scale reconstruction of photosynthetic bacteria.

5. **Study of the proton flux exchange in *Synechocystis***

Changes in environmental conditions, such as temperature, pH, osmolarity, carbon source and electron donators, affect the internal pH as well as energy generation. The cells have to regulate the internal pH by secreting or consuming protons in order to maintain energy homeostasis. The estimation of proton secretion and consumption associated with both cellular growth and metabolism can provide new insights into the metabolism of the target microorganism and can be used to further validate the model. In order to study the proton flux exchange in *Synechocystis*, the growth rate under autotrophic (using CO_2 and HCO_3 as *Ci* source, autotrophic$_{CO2}$ and autotrophic$_{HCO3}$ respectively), mixotrophic and heterotrophic conditions was computed as a function of the proton flux exchange (Fig. S8). Our analysis revealed that the growth rate was strongly dependent on active proton uptake in all the conditions tested. While

the mixotrophic and autotrophic$_{CO2}$ conditions were slightly more sensitive to proton exchange compared to the heterotrophic condition, the predicted growth rates exhibited similar behavior, suggesting that light availability and photosynthetic activity have a modest impact on proton exchange (Fig. S8). Under autotrophic$_{HCO3}$ conditions, proton uptake was found to be strictly necessary for growth and higher medium alkalinization was predicted (Fig. S8). Interestingly, the predicted proton uptake and subsequent medium alkalization were in agreement with the basic medium reported in *Synechocystis* cultures grown under autotrophic conditions (up to pH 10.9) (9, 47). The key reason is that the H^+ consumed in the conversion of HCO_3^- to CO_2 in the carboxysome by carbonic anhydrase leads to an accumulation of OH^- inside the cell that will need to be neutralized by H^+ uptake from the external medium (9). In summary, our analysis is an example of how both the internal proton balancing and the external pH can be predicted by using a completely mass and charge balanced model. In addition, our data highlights that the main factor that drives the proton exchange mechanism in a photosynthetic organism is the carbon source rather than the light availability. The former observation has previously been made for other non-photosynthetic organisms (48).

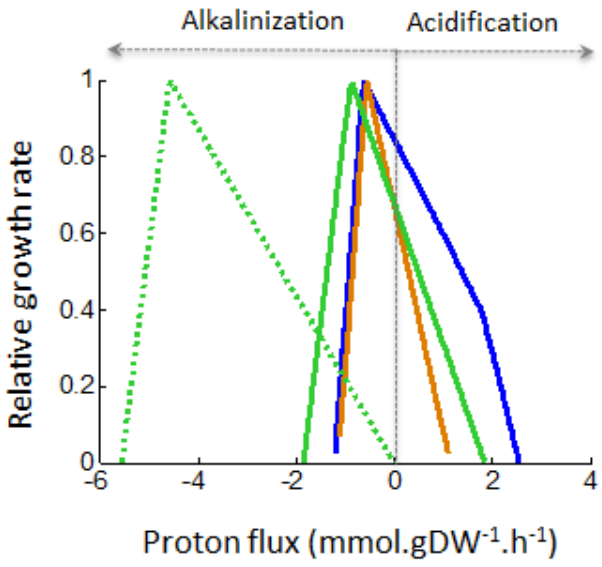

Figure S8. Effect of proton exchange on predicted growth rate. The exchange of protons between the cell and the medium was varied from -6 to 4 mmol.gDW^{-1}.h^{-1} and the relative growth rate was computed under heterotrophic (blue line), mixotrophic (orange line) and autotrophic conditions, using CO_2 (green solid line) and HCO_3 (green dots line) as inorganic carbon, respectively.

6. Metabolic robustness and gene essentiality study of *i*JN678

We studied the minimum number of genes required to sustain growth under autotrophic, mixotrophic and heterotrophic conditions by using gene essentiality analysis (see Supplementary Methods (49, 50)). While 350 genes were found to be essential in the autotrophic condition, significantly fewer genes were predicted to be essential in the heterotrophic and mixotrophic conditions: 261 and 259 respectively (Fig S9*A*). A core of 259 genes was predicted to be essential in all of the conditions, while 91 genes were predicted to be essential only under autotrophic conditions, and two genes only under heterotrophic conditions (Fig. S9*B*). Genes mainly involved in the biosynthesis of lipids, amino acids, photosynthetic pigments, purines and pyridines, as well as other biosynthetic pathways, were predicted to be lethal in all conditions (Dataset S5). In the absence of a systematic gene essentiality analysis in *Synechocystis*, we used the *Synechocystis* mutant collection available in cyanomutant (51) (http://genome.kazusa.or.jp/cyanobase/mutants/) to validate our predictions. A total of 190 genes included in *i*JN678 are present in cyanomutant, of which 44 and 41 have been predicted as essential and non-essential genes respectively (Fig. S9*C,* Dataset S5). Excluding mutants for which non-specific phenotype has been reported; our gene essentiality analysis correctly predicts 79% of the phenotypes described in Cyanomutant (two-sided p-value of Fisher's exact test is less than 10^{-3}). However, we found a significant false positive rate (21%). These are genes that are predicted as essential *in silico* but are non-essential *in vivo* (Fig. S9*C*). Many of these false positives were imposed by detailed biomass objective functions, which require the synthesis of several photosynthetic pigments and lipids. For example, the gene slr008, which encodes for a β-carotene ketolase involved in the synthesis of echinenone, was predicted to be essential. Yet this mutant strain was unable to synthesize echinenone, a metabolite included in our BOF reactions, and its cell viability was not compromised *in vivo* (52), which strongly suggests a high flexibility in the composition of photosynthetic pigments in *Synechocystis* (53). Another group of false positives included genes that were involved in the uptake of metal ions. This suggests that alternative metal transport systems may be present in *Synechocystis* and is in agreement with the high number of putative metal and ion-transporter systems encoded in its genome (Fig. S2). These disparities provide an interesting target for knowledge discovery in the role of photosynthetic pigments as well the metal uptake systems in *Synechocystis*.

Only two genes were found to be essential in the heterotrophic condition (Fig. S9*B,* Dataset S5): *glcP* (sll0771) and *glk* (sll0593). These genes are involved in the first two steps of glucose metabolism, i.e., glucose transport across the inner membrane and its subsequent phosphorylation, producing glucose-6-phosphate. Interestingly, these two genes were reported as essential *in vivo* under the same conditions (27, 54).

On the other hand, most of the 91 essential genes in *Synechocystis* found under autotrophic conditions (Dataset S5) were involved in the photosynthetic machinery, which is in agreement with previous reports (55, 56). In addition, other essential genes were found in the non-oxidative branch of pentose phosphate pathway (Calvin cycle). It is important to note that while glucose is funneled to the pentose phosphate pathway, deletion of genes such as *rpe* (sll0807), *tpi* (sll0783) and *pgk* (slr0394) were only predicted to be lethal under autotrophic conditions. Synthetic lethality has been used as a measure of the robustness of metabolic networks (57). It is associated with gene products, which i) are interchangeable (isoenzymes), ii) act in the same essential pathway, or iii) operate in separate pathways with redundant and/or complementary essential functions. According with the essential genes analysis, a higher number of synthetic lethal genes were predicted under heterotrophic conditions, 234 against only 158 synthetic lethal genes predicted under autotrophic conditions. (Fig. S9*A*). Taken together, these results suggest reduced metabolic robustness under genetic perturbations in *Synechocystis*, especially under autotrophic conditions.

A

	Essential	Synthetic Lethal	Non-essential
Autotrophic	350	158	170
Mixotrophic	259	274	145
Heterotrophic	261	234	183

B

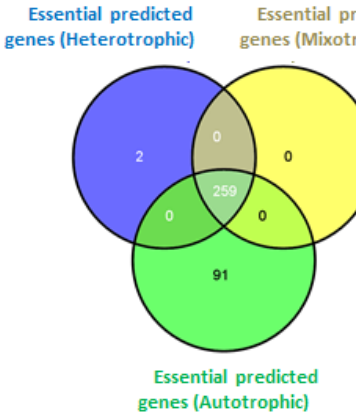

C

In vivo gene essentiality	In silico gene essentiality: essential	In silico gene essentiality: not essential
essential	8 (true positive)	0 (false negative)
not essential	11 (false positive)	32 (true negative)
	25 (ND)	9 (ND)

Figure S9. Gene essentiality and synthetic lethality analysis of *Synechocystis*. (A) Essentiality and synthetic lethality analysis in the different growth conditions. (**B)** Comparison of essential genes under heterotrophic (blue), mixotrophic (yellow) and autotrophic (green) conditions. Venn diagrams were generated by using Venny (58). **(C)** *In vivo*/*in silico* comparison of the core essential and non-essential genes. ND represents those knock-outs included in Cyanomutant but with unknown phenotype or segregation state.

7. **Analysis of the heterotrophic metabolism of *Synechocystis***

The analysis of the genes encoding for transporters suggested that the hetero- and mixotrophic metabolisms have a more important role in *Synechocystis* than previously thought (Fig. S2). The culture of photosynthetic organism under mixo- and heterotrophic conditions have many advantages organisms amount others, higher efficiency and lower cost in conventional microbial fermenters (59). This fact led us to carry out an extensive analysis of the hetero- and mixotrophic metabolisms of *Synechocystis*. Thus, we tested each metabolite that has an associated transport reaction as carbon and nitrogen sources in presence of light (mixotrophic) and in the dark (heterotrophic) (Table S4). The growth predictions suggest a broader heterotrophic metabolism than we expected for a facultative heterotrophic microorganism. *i*JN678 was able to grow heterotrophycally on several organic compounds besides glucose, including fructose, pyruvate, acetate, fumarate, succinate, citrate, oxoglutarate and malate (Table. S4). In addition, some amino acids such as alanine, glutamine and serine under mixotrophic conditions, together with glutamate under both mixo- and heterotrophic conditions, completed the list predicted carbon sources. It is well known that *Synechocystis* is able to use several organic compounds as nitrogen sources instead of nitrate or ammonium (23). Our analysis confirmed that arginine, urea and cyanate were efficient nitrogen sources. In addition, several other amino acids such as alanine, glycine, glutamate, glutamine and serine were predicted here as potential nitrogen sources for *Synechocystis* (Table S4).

Metabolite	Mixotrophic *(In silico/In vivo)*	Chemoheterotrophy (*In silico/In vivo*)	Mixotrophic (*In silico/In vivo*)	Chemoheterotrophy (*In silico/In vivo*)
Glucose	(+/+)[60]	(+/+)[60]	(-/-)	(-/-)
Fructose	(+/±)[60, 61]	(+/±)[60, 61]	(-/-)	(-/-)
Acetate	(+/+)[28]	(+/+)[28]	(-/-)	(-/-)
Fumarate	(+/ND)	(+/ND)	(-/-)	(-/-)
Succinate	(+/ND)	(+/ND)	(-/-)	(-/-)
Citrate	(+/+)[28]	(+/+)[28]	(-/-)	(-/-)
Oxoglutarate	(+/ND)	(+/ND)	(-/-)	(-/-)
Malate	(+/+)[28]	(+/+)[28]	(-/-)	(-/-)
Pyruvate	(+/+)[28, 29]	(+/±)[28, 29]	(-/-)	(-/-)
Alanine	(+/ND)	(-/ND)	(+/ND)	(+/ND)
Arginine	(-/-)[23]	(-/-)[23]	(+/+)[23]	(+/+)[23]
Glycine	(-/-)[23]	(-/-)[23]	(+/ND)	(+/ND)
Glutamate	(+/ND)	(+/ND)	(+/+)[23]	(+/ND)
Glutamine	(+/ND)	(-/ND)	(+/+)[23]	(+/ND)
Histidine	(-/ND)	(-/ND)	(-/-)[23]	(-/-)[23]
Leucine	(-/ND)	(-/ND)	(-/-)[23]	(-/-)[23]
Lysine	(-/ND)	(-/ND)	(-/-)[23]	(-/-)[23]
Proline	(-/ND)	(-/ND)	(-/-)[23]	(-/-)[23]
Serine	(+/ND)	(-/ND)	(+/ND)	(+/ND)
NO_3^{2-}	(-/-)	(-/-)	(+/+)[23]	(+/+)[23]
NH_4^+	(-/-)	(-/-)	(+/+)[23]	(+/+)[23]
Urea	(-/-)	(-/-)	(+/+)[23]	(+/+)[23]
Putrescine	(-/-)[62, 63]	(-/-)[62, 63]	(-/-)[62, 63]	(-/-)[62, 63]
Spermidine	(-/-)[62, 63]	(-/-)[62, 63]	(-/-)[62, 63]	(-/-)[62, 63]
Cyanate	(-/-)	(-/-)	(+/+)[23]	(+/+)[23]
Glucosylglycerol	(-/-)[64, 65]	(-/-)[64, 65]	(-/-)	(-/-)
Sucrose	(-/-)[64, 65]	(-/-)[64, 65]	(-/-)	(-/-)

Table S4. Comparisons of *in silico* growth predictions and *in vivo* experimental data. (+) growth predicted / growth experimentally reported. (-) no growth predicted / no growth experimentally reported. (±) contradictory experimental reports found. ND condition not tested experimentally. Experimental references are indicates.

Metabolite	**Mixo**	**Hetero**	**Metabolite**	**Mixo**	**Hetero**

Metabolite	Mixo	Hetero	Metabolite	Mixo	Hetero
Glucose	1	1	L-erythro-4-Hydroxyglutamate	1	0.784
4-Aminobutanal	0.899	1.056	Succinic semialdehyde	1	0.894
4-Aminobutanoate	0.899	0.918	L-Glutamate 5-semialdehyde	1	0.931
Aspartate	0.899	0.422	Galactose	1	1
Glycolaldehyde	1.001	0.972	(R)-Glycerate	1.001	0.853
D-Alanyl-D-alanine	0.599	0	Glycolate	1.001	0.8
D-Glyceraldehyde	1.001	0.981	D-Lactate	1.001	0.885
Glycerol	1.001	1.123	L-1-Pyrroline-3-hydroxy-5-carboxylate	1	0.979
Ethanol	1.001	0.992	Hydroxypyruvate	1.001	0.733
Acetaldehyde	1.001	0.768	D-Lactaldehyde	1.001	0.992
N(omega)-(L-Arginino)succinate	0.36	0.208	Maltose	1	0.999
Oxaloacetate	1	0.586	Methylglyoxal	1.001	0.872
Formate	0.999	0	Ornithine	0.36	0.424
4-Hydroxy-2-oxoglutarate	1	0.714	1-Pyrroline-5-carboxylate	1	0.944
Glyoxylate	1.001	0.564	D-Ribose	1	1
Deoxyribose	1	0.982	Oxalate	1.001	0

Table S5. Potential new carbon sources for *Synechocystis*. For the evaluation of the new carbon sources, a cytoplasmatic sink reaction for each internal metabolite was introduced in the model and the growth rate in the presence (mixotrophic) and absence (heterotrophic) of light was computed. An uptake rate of 1 mmol.gDW^{-1}.h^{-1} was used. The growth rate relative to glucose is also shown.

In order to complete our analysis regarding the heterotrophic metabolism in *Synechocystis,* we tested the ability of *i*JN678 to grow each of the included internal metabolites as sole carbon source under hetero- and mixotrophic conditions (see Supplementary Methods). This approach could lead to the discovery of new carbon sources based on the metabolic capabilities of *Synechocystis* that were included in *i*JN678 despite missing transport reactions (e.g., due to missing annotation). 31 new carbon sources were predicted (Table S5), including storage polymers such as aspartate (a cyanophycin derivative); carbohydrates such as maltose, galactose, D-ribose and deoxyribose; organic acid derivatives from the glutamate metabolism, such as succinic semialdehyde, hydroxypyruvate, etc.; as well as other compounds, such as glycerol, glycolate, glyoxylate, and lactate (Table S5).

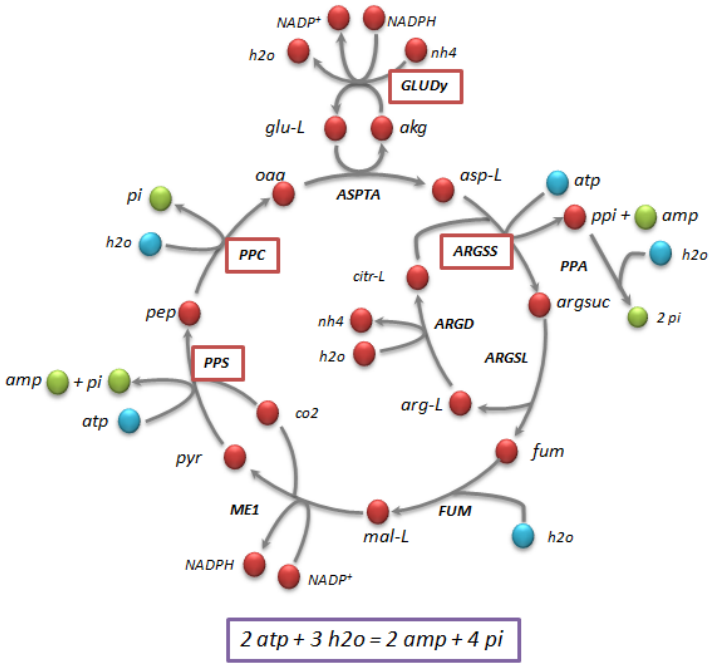

Figure S10. Futile metabolic cycle proposed for ATP/ADP balancing in *Synechocystis under* CLS. Abbreviations for reactions and metabolites are listed in Dataset S1. In red, metabolites produced and consumed. In blue, only metabolites consumed and in green, only metabolites produced. Reactions that have been reported up-regulated under high light and/or low CO_2 are shown in red boxes. The net reaction of the cycle is also indicated.

Supplementary Methods

1. Metabolic reconstruction

The first draft of the *Synechocystis* network was constructed according to the procedure given in Thiele and Palsson (14) and was based on the annotated genome sequence (66) as well as the genomic information available in specific databases, such as Cyanobase (51) and CYORF (http://cyano.genome.jp/). Other online databases, e.g., KEGG (67), METACYC (68) and BRENDA (69), were extensively used as well. Finally, we took advantage of previously published metabolic models of *Synechocystis* (18, 19, 35, 36) and of the biochemical information found in cyanobacteria-specific books (70) and general biochemical textbooks. The resulting first draft accounted for the core metabolism of *Synechocystis,* including the Calvin cycle, glycolysis, the incomplete TCA cycle, the pentose-phosphate pathway, amino-acid, nucleotide and cofactor biosynthetic pathways, as well as other minor pathways. The initial draft was subsequently enhanced by including exclusive pathways to define the identity signatures of *Synechocystis*;

thus, a detailed representation of the photosynthetic apparatus, carbon dioxide fixation, synthesis of photosynthetic pigments, specific fatty acids, and storage polymers such as glycogen, cyanophycin and polyhydroxybutyrate were incorporated. A literature search also led to an extension of the initial reactions list, including the recently reported branches of the photorespiration pathway (10) as well as new genes involved in chlorophyll biosynthesis such as slr1790 (71). The network was subject to iterative gap-filling.

The initial analysis revealed incomplete biosynthetic pathways for several amino acids (e.g., glycine, serine, methionine, and cysteine) and cofactors (e.g., thiamine, folic acid). After verification that the respective biosynthetic products can be synthesized by *Synechocystis*, we filled the gaps based on genes present in phylogenetically close organisms. For example, the cysteine biosynthesis pathway was completed using homoserine O-trans-acetylase (EC 2.3.1.31) and O-acetyl-L-homoserine acetate-lyase (EC 2.5.1.49), which are postulated to be present in other cyanobacteria (http://genome.kazusa.or.jp/cyanobase). Substrates and cofactors, charged formulas for each metabolite, reaction directionality and stoichiometry, information for gene and reaction localization as well as gene-protein-reaction (GPR) associations for each reaction were carefully revised based on the available information for *Synechocystis* or phylogenetically close cyanobacteria. For instance, the succinate dehydrogenase complex (SDH, EC 1.3.99.1), which is described traditionally as a reversible reaction and FAD-dependent, was included in our reconstruction as an irreversible reaction, plastoquinone (PQ) dependent, and placed both in the thylakoid and cytoplasmatic membranes on the basis of experimental data on *Synechocystis* (1, 30). A confidence score was associated with every reaction included in the reconstruction. The score was based on the available evidence for its presence in the *Synechocystis* metabolic network (14). Biochemically characterized enzymes in *Synechocystis* received a confidence score of 4. If genetic knockout information or physiologic evidence was available, a score of 3 was given. A score of 2 was assigned to reactions for which indirect evidence or sequence homology information was available. Multiple types of evidence result in a cumulative confidence score (14). Finally, during gap-filling and evaluation of the network functionality (e.g., biomass precursor production) some reactions were added with a confidence score of 1 (Fig. S3). The complete sets of reactions and metabolites included in the model are given in Dataset S1.

2. Biomass reactions formulation

The biomass reaction accounts for all known biomass constituents and their fractional contribution to the overall cellular biomass (33). A detailed and precise biomass reaction is needed for realistic metabolic network analysis. We formulated the *Synechocystis* biomass reaction according to the procedures given in (14, 33, 72). The fractions corresponding to the main biosynthetic blocks, proteins (51%), carbohydrates (19%), lipids (10%), RNA (17%) and DNA (3%) were based on experimental data (18). The relative fraction of each precursor from protein and nucleic acid blocks was estimated from the genome sequence (14). The relative fraction of each fatty acid was taken from experimental values reported in (16), the composition of glycogen from (73) and the photosynthetic pigments from (53, 74, 75). Finally, the relative fraction of peptidoglycan and soluble pool metabolites was taken from experimental data reported for *Synechocystis* and other Gram-negative bacteria (76, 77).

The energy maintenance, in the form of ATP, for auto-, hetero- and mixotrophic conditions was taken from (18). The relative fraction of growth-associated ATP maintenance reaction (GAM), which accounts for the energy necessary to replicate a cell (e.g., energy required for macromolecular synthesis) and the non-GAM reaction (NGAM), which represents NGAM requirements to maintain other cellular functions (e.g., turgor pressure) was taken from the *E. coli* biomass reaction (72). The phosphate bonds were accounted for by adding ATP hydrolysis to the biomass reaction (x ATP + x H2O → x ADP + x Pi + x H^+). With the exception of the presence of glycogen in the autotrophic biomass reaction and different energy maintenance requirements (18), the three different biomass reactions for autotrophic, mixotrophic, and heterotrophic conditions have a similar composition. A detailed description of the *i*JN678's biomass reactions is depicted in Dataset S3.

3. **Conversion of the reconstruction into a mathematical model**

The conversion of a reconstruction into a mathematical model has been described in detail elsewhere (14). All flux rates, v_i are given in mmol/g_{DW}/h, except biomass formation, which is given in h^{-1}.

4. **Analysis of metabolic flux**

Numerous mathematical tools have been developed to study metabolic network properties *in silico* (see (78) for a review). Many of the tools rely on (linear) optimization to calculate the property of interest, e.g., the maximal possible growth rate of a metabolic network under a given set of environmental constraints.

In flux balance analysis (FBA**)** (79), a metabolic network is framed as a linear programming (LP) problem and a specific cellular objective such as the growth rate or substrate secretion is maximized or minimized. The principal sets of constraints in FBA are those imposed by the steady-state mass conservation of metabolites in the system. The LP is formulated as follows:

maximize $c^T v$ (objective function)

subject to $S \cdot v = 0$

$v_{i,\min} \leq v_i \leq v_{i,\max}$ for all $i = 1, \ldots, n$ reactions,

where S is the m x n stoichiometric matrix, c is the objective function vector, v is a vector of reaction fluxes, $v_{i,\max}$ is the maximal capacity for reaction i, and $v_{i,\min}$ is the minimal capacity for reaction i.

Flux variability analysis (FVA) (80) is used to find the minimum and maximum flux for reactions in the network while maintaining some state of the network. FVA requires the solution of $2n$ linear optimization problems, two for each reaction, $i = 1,\ldots,n$

$\max/\min_v v_i$

Subjet to $S \cdot v = 0$

$c^T v \geq \gamma Z_0$

$v_{i,\min} \leq v_i \leq v_{i,\max}$

where $Z_0 = c^T v_0$ is the optimal solution to the FBA problem above (typically the maximum growth rate) and γ is a parameter that controls whether the analysis is done w.r.t. suboptimal network states ($0 \leq \gamma < 1$) or to the optimal state ($\gamma = 1$). FVA was used in our experiments to find the minimum and maximum flux through each reaction while supporting 99% of the maximal growth rate ($\gamma = 0.99$).

All computational simulations were performed using the COBRA toolbox (81) in the Matlab environment (The MathWorks Inc., Natick, MA). The GNU Linear Programming Kit (GLPK) (http://www.gnu.org/software/glpk) and TomLab (Tomlab Optimization Inc., San Diego, CA) were used to solve the linear and quadratic optimization problems respectively.

5. Formulation of *i*BG-11 minimal medium

An *in silico* BG-11 minimal medium was simulated on the basis of the composition of the BG-11 minimal medium routinely used for *Synechocystis* cultures (82), which contains per liter: $CaCl_2.2H_2O$ 36 mg; $NaNO_3$ 1.5 g; K_2HPO_4 40 mg; $MgSO_4.7H_2O$ 75 mg; $CuSO_4.5H_2O$ 0.079 mg; $Na_2MoO_4.2H_2O$ 0.39 mg; H_3BO_3 2.86 mg; $EDTANa.2H_2O$ 1 mg; $NaCO_3$ 0.02 g; $NH_4Fe(C_6H_5O_7)$ 0.006 g; $MnCl_2.4H_2O$ 1.81 mg; $ZnSO_4.7H_2O$ 0.222 mg; $Co(NO_3)_2.6H_2O$ 0.049 mg. By assuming that these concentrations do not impose a growth restriction, the external metabolites Co^{2+}, Fe^{2+}, Fe^{3+}, H^+, H_2O, Na^{2+}, Ni^{2+}, Cu^{2+}, Zn^{2+}, Ca^{2+}, CO_2^-, HCO_3^-, Mg^{2+}, Mn^{2+}, Mo^{2+}, K^{2+}, O_2, NO_3^{2-}, P_i and SO_4 were allowed to freely enter and leave the network. Unconstrained uptake/secretion is represented in *i*JN678 by lower/upper bounds of -/+ 10^3 mmol/gDW/h. In each individual simulation, all other external metabolites were only allowed to leave the system by constraining their exchange fluxes between [0, 10^3] mmol/gDW/h, unless otherwise noted.

6. Simulation constraints

Growth rate performance. The following simulations were carried out in the *i*BG-11 minimal medium. Autotrophic metabolism was simulated by constraining the CO_2 or HCO_3 exchange fluxes between [-3.7, 10^3] mmol/gDW/h in accordance with the maximum CO_2 uptake rate estimated by (18). The photon uptake rate was constrained between [-100, 0] mmol/gDW/h which corresponds to maximum irradiation of 24 to 39 $\mu E\ m^{-2}.s^{-1}$ for photosynthesis yields of 6% or 4.6% respectively (40) . Heterotrophic metabolism using glucose as the sole carbon source was simulated by constraining its exchange flux between [-0.85, 10^3] mmol/gDW/h in accordance with the glucose uptake rate reported by (37) and photon uptake to 0 mmol/gDW/h. Mixotrophic metabolism was simulated by constraining the uptake rates of CO_2 (HCO3), glucose and photons to 3.7, 0.38 and 100 mmol/gDW/h respectively. In the experiments involving internal flux distribution and growth rate predictions, mixotrophic conditions were simulated by constraining the *Ci* uptake rate to 0 according the culture conditions described by Yang et al (37).

Study of proton flux exchange in Synechocystis. The relative growth rates under autotrophic conditions using CO_2 and HCO_3, as well as under the mixo- and heterotrophic conditions described above, were computed as a function of proton flux exchange by constraining the H^+ exchange fluxes between [-6, 4] mmol/gDW/h.

Expansion of the known array of carbon- and nitrogen sources which support growth. For the evaluation of potential carbon sources, the glucose uptake rate from the heterotrophic and mixotrophic conditions was constrained to 0 and the exchange fluxes for each potential carbon source *i* were changed between $v_{i,\min} \geq -1$ and $v_{i,\max} \geq 1000$ mmol/gDW/h. For the evaluation of potential nitrogen sources, the NO_3 uptake rate was set to zero and glucose used as the sole carbon source in heterotrophic and mixotrophic simulations. The potential nitrogen sources were allowed to enter the network freely (lower bounds of -10^3). A growth rate of at least 10% of the growth obtained with glucose and NO_3 was taken as an indication of growth.

For the evaluation of potential new carbon sources, the glucose uptake rate from the heterotrophic and mixotrophic simulations was constrained to zero and a cytoplasmatic sink reaction for each metabolite included in the reconstruction was added to the network. A lower bound of -1 mmol/gDW/h for each sink reaction was used, and the relative growth rate by carbon atom compared with hetero- or mixotrophic growth at the expense of glucose (lower bound of -1) was computed.

7. Gene essentiality and synthetic lethal analysis

The minimum number of genes required to sustain growth was studied under autotrophic, mixotrophic and heterotrophic conditions using the simulation procedure from (49, 50). A single simulation starts with a full network and selects a gene at random. If removal of this particular gene results in a viable network, the gene is permanently removed. The process is repeated for all the genes in the network. The remaining genes are essential for network survival. On the basis of 1000 simulation runs, sets of always-present genes (essential), sometimes-present genes (synthetic lethal) and never-present (nonessential) were identified. The network viability criterion was a minimum growth rate of 10% of the wild-type growth. For autotrophic growth, the carbon dioxide uptake was set to 3.7 mmol/gDW/h and the photon uptake to 100

mmol/gDW/h. For mixotrophic growth, glucose was added to the system by allowing an uptake corresponding to 0.85 mmol/gDW/h. For heterotrophic growth, light uptake was set to zero and glucose uptake to 0.85 mmol/gDW/h.

8. A simplified model used for photosynthesis analysis

The photosynthetic apparatus modeling of *Synechocystis* in *i*JN678 accounts for equivalent reactions placed in different compartments as well as the broad use of alternative cofactors based on experimental evidence (Fig. S1, Dataset S1). In order to simplify the photosynthesis analysis, only photosynthetic reactions placed in the thylakoid membrane were allowed, and only one electron carrier was allowed. For this, the following constraints were applied:

- Since the blue copper protein plastocyanin (PC) and the heme protein cytochrome c6 (CytC) perform the same function in the photosynthetic electron-transport chain (39, 83), only PC was allowed as a soluble electron carrier, accepting electrons from cytochrome b_6f to reduce PSI. Thus, the fluxes across reactions CBFC2, PSI_2 and CYO1b_syn were constrained to zero (Fig. S1, Dataset S1).
- The NDH-1 complex can accept electrons from both NADPH and NADH (84). Since a specific NADH dehydrogenase was included in the reconstruction (NDH-2), only NADPH was allowed as an electron donator to the NDH-1 complex in order to simplify the analysis. For this, the fluxes across reactions NDH1_2u and NDH1_2p were constrained to zero (Fig. S1, Dataset S1).
- Only the reactions placed in the thylakoid membrane were allowed. The fluxes across reactions NDH1_1p, CYO1b2pp_syn, CYO1bpp_syn, CBFCpp and CYTBDpp were therefore constrained to zero (Fig. S1, Dataset S1).
- The reaction ferredoxin $NADP^+$ reductase (FNOR) (EC: 1.18.1.2) was assumed to be irreversible under autotrophic conditions.

The following COBRA commands (14, 85) were used in order to apply the constraints to the model.

```
 initCobraToolbox
model = xls2model ('Dataset S1.xlsx');
```

%Autotrophic conditions

```
model = changeObjective (model, 'Ec_biomass_SynAuto');
model = changeRxnBounds (model, 'EX_photon(e)', -100,'l');
model = changeRxnBounds (model, 'EX_glc(e)', 0,'l');
model = changeRxnBounds (model, 'EX_hco3(e)',-3.7,'l');
%Computing growth rate
sol=optimizeCbModel(model)
%sol = f: 0.0884
```

%Simplified photosynthetic model

```
 %Constraining cytochrome c6-dependent reactions.
model = changeRxnBounds(model, 'CBFC2',0, 'b');
model = changeRxnBounds(model, 'PSI_2',0, 'b');
model = changeRxnBounds(model, 'CYO1b_syn',0, 'b');

 %Constraining NADH-dependent reactions.
model = changeRxnBounds(model, 'NDH1_2u',0, 'b');
model = changeRxnBounds(model, 'NDH1_2p',0, 'b');

 %Constraining peryplasmatic reactions.
model = changeRxnBounds(model, 'NDH1_1p',0, 'b');
model = changeRxnBounds(model, 'CYO1b2pp_syn',0, 'b');
model = changeRxnBounds(model, 'CYO1bpp_syn',0, 'b');
model = changeRxnBounds(model, 'CBFCpp',0, 'b');
model = changeRxnBounds(model, 'CYTBDpp',0, 'b');

 %Assumed irreversibility of ferredoxin NADPH reductase under autotrophic
conditions.
model = changeRxnBounds(model, 'FNOR',0, 'l');
 %Assumed no excretion of CO2 under autotrophic conditions
model = changeRxnBounds (model, 'EX_co2(e)',0,'u');
```

%Model constraints applied to generate Figure 1

By using the simplified photosynthetic model, we constrained to zero the lower and upper bounds of the all AEF pathways identified.

%Building a model lacking AEF pathways

```
 %Constraining NDH-1
model = changeRxnBounds(model, 'NDH1_1u',0, 'b');
```

```
%Constraining NDH-2
model = changeRxnBounds(model, 'NDH2_syn',0, 'b');
%Constraining NDH-1₃. NDH-1₄ is homologous reaction to NDH-13 but placed in
periplasm.
model = changeRxnBounds(model, 'NDH1_3u',0, 'b');
%Constraining FQR
model = changeRxnBounds(model, 'FQR',0, 'b');
%Constraining CYO
model = changeRxnBounds(model, 'CYO1b2_syn',0, 'b');
%Constraining CydBD
model = changeRxnBounds(model, 'CYTBDu',0, 'b');
%Constraining H2ase
model = changeRxnBounds(model, 'H2ASE_syn',0, 'b');
%Constraining MEHLER
model = changeRxnBounds(model, 'MEHLER',0, 'b');
```

Photorespiratory metabolism was constrained by constraining the oxygenic and carboxygenic activity of RuBisCO to minimum flux, which sustains maximum growth rate (0.0884).

% Building a model with the photorespiratory metabolism constrained

```
    %Costraining Carboxygenic activity of RuBisCO
model = changeRxnBounds(model, 'RBPC',4.30987, 'u')
    %Constraining Oxygenic activity of RuBisCO
model = changeRxnBounds(model, 'RBCh',0.2045310, 'u');
```

Computation of the functional states exhibited by *i*JN678 when employing one AEF at a time was done by restoring the original bounds of each AEF pathway studied (Fig. 1*C-I*).

9. Robustness analysis of photosynthesis.

When FBA is applied to metabolic networks there are in general infinitely many flux distributions corresponding to the maximum cellular objective. Which flux distribution is obtained, depends on the particular LP solver used. To investigate how the presence of such alternate solutions affects our results, we computed the minimum and maximum possible flux through each of the reactions presented in Fig. 1 with fixed light uptake and growth rate (Fig. S11). With the exception of the FNR reaction and photorespiration in the CLS, there was essentially no variation which suggests that our results are robust to different attainable solutions. The large variation in FNR (which produces one mole of NADPH from 2 moles of reduced ferredoxin) is explained by the fact that multiple reactions included in the model can be used for converting between reducing equivalents. For instance, in the NH_4 fixation pathway, the reactions GLUSx, GLUDy, GLMS_syn and GLNS can work cooperatively, producing NAD(P)H from ferredoxin thus partially overcoming the role of FNR. However, these reactions don't result in net reducing equivalents consumption and they are well regulated *in vivo*. If it is assumed that GLUDy only works in the reverse direction (it is mainly involved in nh4 fixation rather than glutamate dehydrogenation) the variation in FNOR decreases significantly. The small variation in PHOTOR is due to the presence of redundant photo-respiration pathways. In summary, we conclude that our results are robust towards the presence of alternate optima.

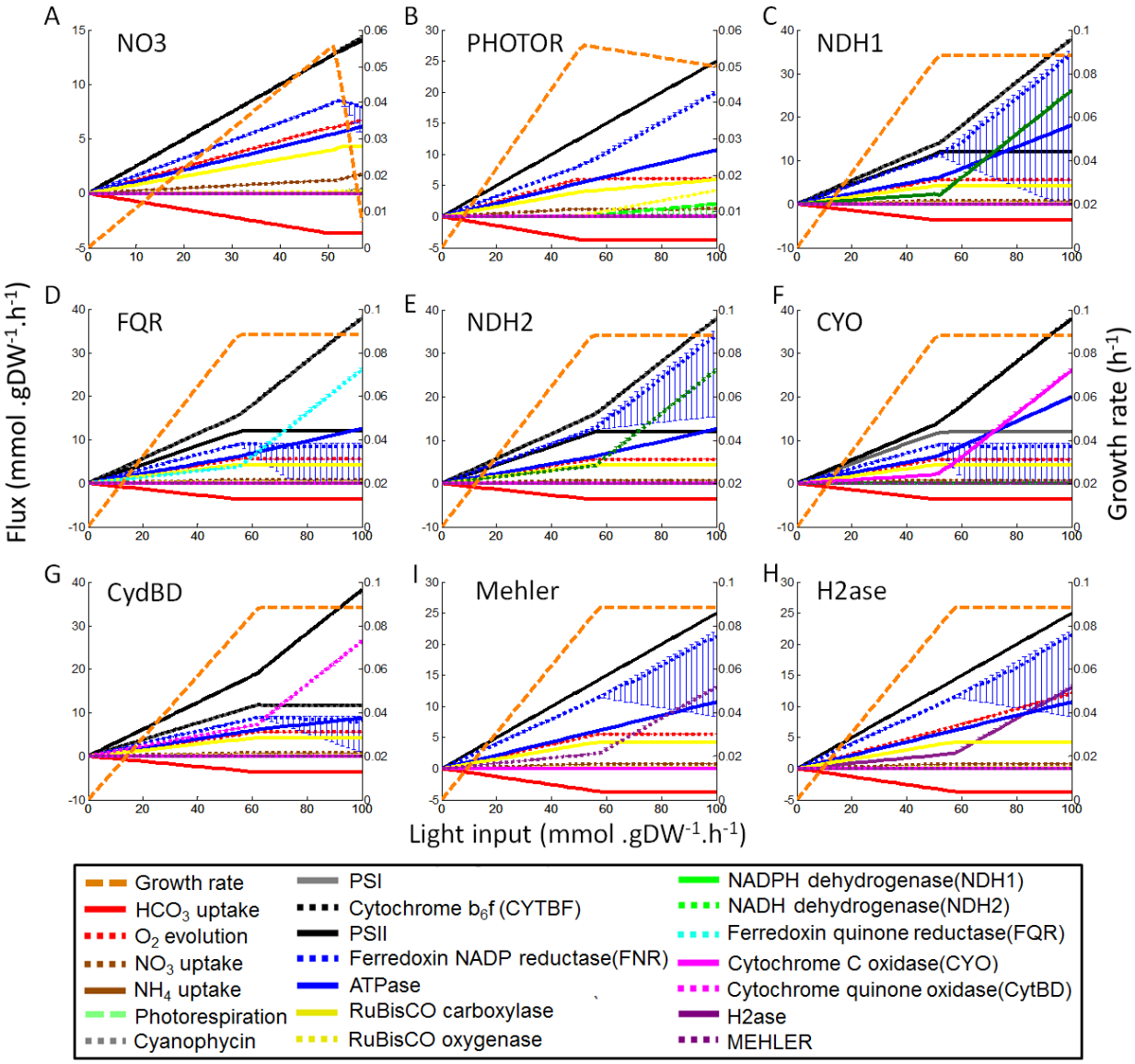

Fig.S11. Robustness analysis of photosynthesis. Impact of *Ci* (i.e., HCO_3^-) and light availability on the autotrophic metabolism of *Synechocystis.* Variability in the functional states found in: **A,** the absence of AEF pathways and photorespiration; **B,** the absence of AEF pathways allowing photorespiration; **C-I**, the presence of one AEF pathway (indicated by the caption in each diagram). The growth rate (orange, right *y*-axis) was computed under autotrophic by using HCO_3^- as *Ci* carbon source (uptake = 3.7 mmol.gDW^{-1}.h^{-1}) and NO_3 as nitrogen source (unconstrained uptake rate) as a function of light availability by varying the photon uptake rate from 0 to 100 mmol.gDW^{-1}.h^{-1} (*x*-axis). The computed flux rates for each relevant reaction are shown (left, *y*-axis). Vertical bars show the possible flux variability in individual reactions.

10. Estimation of ATP/NADPH ratio

Under non-photorespiratory conditions

The quantification of the photosynthetic parameters exhibited by AEF pathways is extensively detailed in Dataset S6. Briefly, all the reducing power from PSI was taken as NADPH ($Flux_{PSI}$) and 3 x flux across the ATPSu reaction was considered as the total ATP production ($3xFlux_{ATPSu}$) (86).

- NADPH consumption by NDH-1, NDH-1_3, NDH-2, FQR, MEHLER and H2ase

The total NADPH consumed by these pathways was calculated, taking into account that 1 mmol/gDW/h of NADPH is consumed per flux unit across these pathways ($Flux_i$), where i = NDH-1, NDH-1_3, NDH-2, FQR, MEHLER or H2ase.

- Net NADPH levels yield by AEF pathways

The remaining NADPH levels were calculated by subtracting the NADPH consumed from the total NADPH levels produced by PSI.

$Net_{NADPHnp} = Flux_{PSI} - Flux_i$ where $Net_{NADPHnp}$ = net NADPH produced (mmol/gDW/h) under non-photorespiratory conditions.

For CYO and CydBD, the NADPH from PSI was assumed as total NADPH produced, since these reactions accept electrons before passing them to PSI, e.g., from plastocianin/cytochrome c6 and plastoquinone respectively (Fig. S1).

- Net ATP levels yield by AEF pathways

$Net_{ATPnp} = 3xFlux_{ATPSu,}$ where Net_{ATPnp} = net ATP produced (mmol/gDW/h) under non-photorespiratory conditions.

- ATP/NADPH ratio under non-photorespiratory conditions

  $Net_{ATPnp} / Net_{NADPHnp}$

Under photorespiratory conditions

Under photorespiratory conditions, 2 ATP and one NADPH are necessary to produce 1 Glyceraldehyde-3P + 1 CO_2 from two 2-phosphoglycolate (87).

$Flux_{PHOTOR}$ = Fluxes across photorrespiratory pathways (TRSARr or GLYCL, Dataset S1).

Additionally, 3 ATP and 2 NADPH are required for the re-fixing of the CO_2 produced.

- NADPH consumption by photorespiratory pathways

$cNADPH_{ph} = Flux_{PHOTOR}$, where $cNADPH_{ph}$ = NADPH consumed (mmol/gDW/h) under photorespiratory conditions.

- Net NADPH levels yield by photorespiratory pathways

$Net_{NADPHph} = Flux_{PSI} – cNADPH_{ph}$, where $Net_{NADPHph}$ = net NADPH produced (mmol/gDW/h) under photorespiratory conditions.

- ATP consumption by photorespiratory pathways

$cATP_{ph} = 2\ Flux_{PHOTOR}$, where $cATP_{ph}$ is the ATP consumed (mmol/gDW/h) under photorrespiratory conditions.

- Net ATP levels yield by photorespiratory pathways

  $Net_{ATPph} = 3Flux_{ATPSu} – cATP_{ph}$, where Net_{ATPph} = net ATP produced (mmol/gDW/h) under photorespiratory conditions.

- ATP/NADPH ratio under photorespiratory conditions

$Net_{ATPph} / Net_{NADPHph}$

Under extra NO_3 reduction conditions

Five NADPH (ten reduced ferredoxin) and 1 ATP are required to reduce NO_3 to NH_4 and the further fixation of this last compound into glutamine (88). In the absence of AEF pathways and extra reduction, fixation of NO_3 was computed (Fig. 2).

$\Delta Flux_{NOR} = NOR - NOR_{AEF,}$ where $\Delta Flux_{NOR}$ is the increments in the flux across the nitrite reductase (NOR_syn, Dataset S1) under extra NO_3 reduction conditions, NOR the flux across NOR_syn in the absence of AEF pathways and NOR_{AEF} the flux across NOR_syn in the presence of AEF pathways.

- NADPH consumption by extra NO_3 reduction

$cNADPH_{NO3} = 5\ Flux_{NOR}$, where $cNADPH_{NO3}$ = NADPH consumed (mmol/gDW/h) under extra NO_3 reduction conditions.

- Net NADPH levels yield extra NO_3 reduction

$Net_{NADPHNO3}$ = $Flux_{PSI}$ – $cNADPH_{NO3}$, where $Net_{NADPHNO3}$ = net NADPH produced (mmol/gDW/h) under extra NO_3 reduction conditions.

- ATP consumption by extra NO_3 reduction

$cATP_{NO3}$ = $\Delta Flux_{NOR}$, where $cATP_{NO3}$ is the ATP consumed (mmol/gDW/h) under extra NO_3 reduction conditions.

- ATP consumption by cyanophycins biosynthesis (2x DM_cyanophy)

$cATP_{cya}$ = 2x $Flux_{cyan}$, where $cATP_{cya}$ is the ATP consumed (mmol/gDW/h) by cyanophicyns biosynthesis.

- Net ATP levels yield by extra NO_3 reduction

  Net_{ATPNO3} = 3$Flux_{ATPSu}$ – ($cATP_{NO3}$ + $cATP_{cya}$), where Net_{ATPNO3} = net ATP produced (mmol/gDW/h) under extra NO_3 reduction conditions.

- ATP/NADPH ratio under extra NO_3 reduction conditions

Net_{ATPNO3} / $Net_{NADPHNO3}$

11. Sequence data analysis

A homology search with completed cyonabacterial genomes was performed with the BLASTP algorithm (89) at the Cyanobase server (http://genome.kazusa.or.jp/cyanobase). The template proteins used in the analysis of the GABA shunt, TCA cycle and glucose transporter in cyanobacteria were:

- Glutamate decarboxylase (GLUCD) (EC: 4.1.1.15): GadB (b1419) from *E. coli*.
- 4-aminobutyrate aminotransferase (ABTA) (EC: 2.6.1.19): ABAT from *Homo sapiens* (18), PuuE (b1302) and GabT (b2662) from *E. coli*.
- Succinate-semialdehyde dehydrogenase (SSALyr) (EC: 1.2.1.16): GabD (b2661) from *E. coli*.
- 2-oxoglutarate decarboxylase complex (AKGDH): SucA (b0726) and SucB (b0727) from *E. coli*.
- Isocitrate lyase (ICL) (EC:4.1.3.1): AceA (b4015) from *E. coli*.
- Malate synthase (MS) (EC: 2.3.3.9): AceB (b4014) from *E. coli.*
- Glucose transport (GLCt2pp): GlcP (sll0771) from *Synechocystis.*

Supplementary References

1. Cooley JW & Vermaas WFJ (2001) Succinate Dehydrogenase and Other Respiratory Pathways in Thylakoid Membranes of Synechocystis sp. Strain PCC 6803: Capacity Comparisons and Physiological Function. *J. Bacteriol.* 183(14):4251-4258.
2. Ogawa T & Mi H (2007) Cyanobacterial NADPH dehydrogenase complexes. *Photosynthesis Research* 93(1):69-77.
3. Howitt CA & Vermaas WF (1998) Quinol and cytochrome oxidases in the cyanobacterium Synechocystis sp. PCC 6803. *Biochemistry* 37(51):17944-17951.
4. Allen JF (2002) Photosynthesis of ATP--Electrons, Proton Pumps, Rotors, and Poise. *Cell* 110(3):273-276.
5. Howitt C, Cooley J, Wiskich J, & Vermaas W (2001) A strain of *Synechocystis* sp. PCC 6803 without photosynthetic oxygen evolution and respiratory oxygen consumption: implications for the study of cyclic photosynthetic electron transport. *Planta* 214(1):46-56.
6. Yeremenko N*, et al.* (2005) Open Reading Frame ssr2016 is Required for Antimycin A-sensitive Photosystem I-driven Cyclic Electron Flow in the Cyanobacterium Synechocystis sp. PCC 6803. *Plant and Cell Physiology* 46(8):1433-1436.
7. Helman Y*, et al.* (2003) Genes Encoding A-Type Flavoproteins Are Essential for Photoreduction of O2 in Cyanobacteria. *Current Biology* 13(3):230-235.
8. Germer F*, et al.* (2009) Overexpression, Isolation, and Spectroscopic Characterization of the Bidirectional [NiFe] Hydrogenase from Synechocystis sp. PCC 6803. *Journal of Biological Chemistry* 284(52):36462-36472.
9. Price GD, Badger MR, Woodger FJ, & Long BM (2008) Advances in understanding the cyanobacterial CO2-concentrating-mechanism (CCM): functional components, Ci transporters, diversity, genetic regulation and prospects for engineering into plants. *Journal of Experimental Botany* 59(7):1441-1461.
10. Eisenhut M*, et al.* (2008) The photorespiratory glycolate metabolism is essential for cyanobacteria and might have been conveyed endosymbiontically to plants. *Proceedings of the National Academy of Sciences* 105(44):17199-17204.
11. Schäfer L, Vioque A, & Sandmann G (2005) Functional in situ evaluation of photosynthesis-protecting carotenoids in mutants of the cyanobacterium Synechocystis PCC6803. *Journal of Photochemistry and Photobiology B: Biology* 78(3):195-201.
12. DellaPenna D & Pogson BJ (2006) VITAMIN SYNTHESIS IN PLANTS: Tocopherols and Carotenoids. *Annual Review of Plant Biology* 57(1):711-738.
13. Wang F, Jiang JG, & Chen Q (2010) Progress on molecular breeding and metabolic engineering of biosynthesis pathways of C30, C35, C40, C45, C50 carotenoids. *Biotechnology Advances* 25(3):211-222.
14. Thiele I & Palsson BO (2010) A protocol for generating a high-quality genome-scale metabolic reconstruction. *Nat. Protocols* 5(1):93-121.
15. Liu X, Sheng J, & Curtiss III R (2011) Fatty acid production in genetically modified cyanobacteria. *Proceedings of the National Academy of Sciences* 108(17):6899-6904.
16. Okazaki K, Sato N, Tsuji N, Tsuzuki M, & Nishida I (2006) The Significance of C16 Fatty Acids in the sn-2 Positions of Glycerolipids in the Photosynthetic Growth of Synechocystis sp. PCC6803. *Plant Physiol.* 141(2):546-556.

17. Tasaka Y*, et al.* (1996) Targeted mutagenesis of acyl-lipid desaturases in Synechocystis: evidence for the important roles of polyunsaturated membrane lipids in growth, respiration and photosynthesis. *EMBO Journal* 15(23):6416-6425.
18. Shastri AA & Morgan JA (2005) Flux Balance Analysis of Photoautotrophic Metabolism. *Biotechnology Progress* 21(6):1617-1626.
19. Fu P (2009) Genome-scale modeling of *Synechocystis sp*. PCC6803 and prediction of pathway insertion. *Journal of Chemical Technology & Biotechnology* 84:473 - 483.
20. Knoop H, Zilliges Y, Lockau W, & Steuer R (2010) The Metabolic Network of Synechocystis sp. PCC 6803: Systemic Properties of Autotrophic Growth. *Plant Physiology* 154(1):410-422.
21. Montagud A*, et al.* (2011) Flux coupling and transcriptional regulation within the metabolic network of the photosynthetic bacterium *Synechocystis sp*. PCC6803. *Biotechnology Journal* 6(3):330-342.
22. Montagud A, Navarro E, Fernandez de Cordoba P, Urchueguia J, & Patil K (2010) Reconstruction and analysis of genome-scale metabolic model of a photosynthetic bacterium. *BMC Syst Biol* 4(1):156.
23. Luque I & Forchhammer K (2008) Nitrogen Assimilation and C/N Balance Sensing. *The Cyanobacteria. Molecular Biology, Genomics and Evolution*, eds Herrero A & Flores E (Caister Academic Press, Norfolk, UK), pp 335-382.
24. Laudenbach DE & Grossman AR (1991) Characterization and mutagenesis of sulfur-regulated genes in a cyanobacterium: evidence for function in sulfate transport. *J. Bacteriol.* 173(9):2739-2750.
25. Pitt FD, Mazard S, Humphreys L, & Scanlan DJ (2010) Functional Characterization of Synechocystis sp. Strain PCC 6803 pst1 and pst2 Gene Clusters Reveals a Novel Strategy for Phosphate Uptake in a Freshwater Cyanobacterium. *J. Bacteriol.* 192(13):3512-3523.
26. Quintero MJ, Montesinos ML, Herrero A, & Flores E (2001) Identification of Genes Encoding Amino Acid Permeases by Inactivation of Selected ORFs from the Synechocystis Genomic Sequence. *Genome Research* 11(12):2034-2040.
27. Schmetterer G (1990) Sequence conservation among the glucose transporter from the cyanobacterium Synechocystis sp. PCC 6803 and mammalian glucose transporters. *Plant Mol Biol* 14(5):697-706.
28. Koksharova O, Schubert M, Shestakov S, & Cerff R (1998) Genetic and biochemical evidence for distinct key functions of two highly divergent GAPDH genes in catabolic and anabolic carbon flow of the cyanobacterium Synechocystis sp. PCC 6803. *Plant Molecular Biology* 36(1):183-194.
29. Bricker TM*, et al.* (2004) The Malic Enzyme Is Required for Optimal Photoautotrophic Growth of Synechocystis sp. Strain PCC 6803 under Continuous Light but Not under a Diurnal Light Regimen. *J. Bacteriol.* 186(23):8144-8148.
30. Cooley JW, Howitt CA, & Vermaas WFJ (2000) Succinate:Quinol Oxidoreductases in the Cyanobacterium Synechocystis sp. Strain PCC 6803: Presence and Function in Metabolism and Electron Transport. *J. Bacteriol.* 182(3):714-722.
31. Tamber S & Hancock REW (2004) The outer membranes of pseudomonads. *Pseudomonas*, ed Ramos JL (Kluwer Academic, New York), Vol 1, pp 575-601.
32. Reed JL, Vo TD, Schilling CH, & Palsson BO (2003) An expanded genome-scale model of Escherichia coli K-12 (iJR904 GSM/GPR). *Genome Biology* 4(9):R54.51 - R54.52.

33. Feist AM & Palsson BO (2010) The biomass objective function. *Current Opinion in Microbiology* 13(3):344-349.
34. Janssen P, Goldovsky L, Kunin V, Darzentas N, & Ouzounis C (2005) Genome coverage, literally speaking. The challenge of annotating 200 genomes with 4 million publications. *EMBO Rep* 6(5):397-399.
35. Hong SJ & Lee CG (2007) Evaluation of central metabolism based on a genomic database of *Synechocystis* sp. PCC6803. *Biotechnology and Bioprocess Engineering* 12(2):165-173.
36. Navarro E, Montagud A, Fernández de Córdoba P, & Urchueguía JF (2009) Metabolic flux analysis of the hydrogen production potential in Synechocystis sp. PCC6803. *International Journal of Hydrogen Energy* 34(21):8828-8838.
37. Yang C, Hua Q, & Shimizu K (2002) Metabolic flux analysis in *Synechocystis* using isotope distribution from 13C-labeled glucose. *Metab Eng* 4:202 - 216.
38. Emlyn-Jones D, Ashby M, & Mullineaux C (1999) A gene required for the regulation of photosynthetic light harvesting in the cyanobacterium Synechocystis 6803. *Mol Microbiol* 33:1050-1058.
39. Eriksen N, Riisgård F, Gunther W, & Iversen JJL (2007) On-line estimation of O_2; production, CO_2; uptake, and growth kinetics of microalgal cultures in a gas-tight photobioreactor. *Journal of Applied Phycology* 19(2):161-174.
40. Zhu X-G, Long SP, & Ort DR (2008) What is the maximum efficiency with which photosynthesis can convert solar energy into biomass? *Current Opinion in Biotechnology* 19(2):153-159.
41. Foster J, Singh A, Rothschild L, & Sherman L (2007) Growth-phase dependent differential gene expression in *Synechocystis* sp. strain PCC 6803 and regulation by a group 2 sigma factor. *Archives of Microbiology* 187(4):265-279.
42. Shastri AA & Morgan JA (2007) A transient isotopic labeling methodology for 13C metabolic flux analysis of photoautotrophic microorganisms. *Phytochemistry* 68(16-18):2302-2312.
43. Pelroy RA, Rippka R, & Stanier RY (1972) Metabolism of glucose by unicellular blue-green algae. *Arch Mikrobiol* 87(4):303-322.
44. Stal LJ & Moezelaar R (1997) Fermentation in cyanobacteria. *FEMS Microbiology Reviews* 21(2):179-211.
45. Young JD, Shastri AA, Stephanopoulos G, & Morgan JA (2011) Mapping photoautotrophic metabolism with isotopically nonstationary 13C flux analysis. *Metabolic Engineering* 13(6):656-665.
46. Owittrim G & Colman B (1988) Phosphoenolpyruvate carboxylase mediated carbon flow in a cyanobacterium. *Biochem. Cell Biol* 66:93-99.
47. Kim HW, Vannela R, Zhou C, & Rittmann BE (2011) Nutrient acquisition and limitation for the photoautotrophic growth of Synechocystis sp. PCC6803 as a renewable biomass source. *Biotechnology and Bioengineering* 108(2):277-285.
48. Srinivasan K & Mahadevan R (2010) Characterization of proton production and consumption associated with microbial metabolism. *BMC Biotechnology* 10(1):2.
49. Zhang Y*, et al.* (2009) Three-Dimensional Structural View of the Central Metabolic Network of Thermotoga maritima. *Science* 325(5947):1544-1549.
50. Pál C*, et al.* (2006) Chance and necessity in the evolution of minimal metabolic networks. *Nature* 440(7084):667-670.

51. Nakao M, *et al.* (2010) CyanoBase: the cyanobacteria genome database update 2010. *Nucleic Acids Research* 38(suppl 1):D379-D381.
52. Fernández-González B, Sandmann G, & Vioque A (1997) A New Type of Asymmetrically Acting β-Carotene Ketolase Is Required for the Synthesis of Echinenone in the Cyanobacterium Synechocystis sp. PCC 6803. *Journal of Biological Chemistry* 272(15):9728-9733.
53. Lagarde D, Beuf L, & Vermaas W (2000) Increased production of zeaxanthin and other pigments by application of genetic engineering techniques to Synechocystis sp. strain PCC 6803. *Appl Environ Microbiol* 66:64-72.
54. Lee JM, *et al.* (2005) Identification of a glucokinase that generates a major glucose phosphorylation activity in the cyanobacterium *Synechocystis* sp. PCC 6803. *Mol Cells* 19(2):256-261.
55. Astier C, Elmorjani K, Meyer I, Joset F, & Herdman M (1984) Photosynthetic mutants of the cyanobacteria Synechocystis sp. strains PCC 6714 and PCC 6803: sodium p-hydroxymercuribenzoate as a selective agent. *J Bacteriol* 158:659-664.
56. Osiewacz H (1992) Construction of insertion mutants of Synechocystis sp. PCC 6803: Evidence for an essential function of subunit IV of the cytochrome b6/f complex. *Arch Microbiol* 157(4):336-342.
57. Kitano H (2004) Biological robustness. *Nat Rev Genet* 5(11):826-837.
58. Oliveros JC (2007) VENNY. An interactive tool for comparing lists with Venn Diagrams. in http://bioinfogp.cnb.csic.es/tools/venny/.
59. Chen G-Q & Chen F (2006) Growing Phototrophic Cells without Light. *Biotechnology Letters* 28(9):607-616.
60. Anderson SL & McIntosh L (1991) Light-activated heterotrophic growth of the cyanobacterium *Synechocystis* sp. strain PCC 6803: a blue-light-requiring process. *J. Bacteriol.* 173(9):2761-2767.
61. Panda B & Mallick N (2007) Enhanced poly-β-hydroxybutyrate accumulation in a unicellular cyanobacterium, Synechocystis sp. PCC 6803. *Letters in Applied Microbiology* 44(2):194-198.
62. Raksajit W, Mäenpää P, & Incharoensakdi A (2006) Putrescine transport in a cyanobacterium *Synechocystis* sp. PCC 6803. *J Biochem Mol Biol* 39(4):394-399.
63. Raksajit W, Yodsang P, Maenpaa P, & Incharoensakdi A (2009) Characterization of spermidine transport system in a cyanobacterium,synechocystis sp. PCC 6803. *J Microbiol Biotechnol* 19(5):447-454.
64. Hagemann M, Richter S, & Mikkat S (1997) The ggtA gene encodes a subunit of the transport system for the osmoprotective compound glucosylglycerol in Synechocystis sp. strain PCC 6803. *J. Bacteriol.* 179(3):714-720.
65. Mikkat S & Hagemann M (2000) Molecular analysis of the *ggtBCD* gene cluster *Synechocystis* sp. strain PCC6803 encoding subunits of an ABC transporter for osmoprotective compounds. *Archives of Microbiology* 174(4):273-282.
66. Kaneko T, *et al.* (1996) Sequence Analysis of the Genome of the Unicellular Cyanobacterium Synechocystis sp. Strain PCC6803. II. Sequence Determination of the Entire Genome and Assignment of Potential Protein-coding Regions. *DNA Research* 3(3):109-136.
67. Kanehisa M, *et al.* (2006) From genomics to chemical genomics: new developments in KEGG. *Nucl Acids Res* 34(suppl_1):D354 - 357.

68. Caspi R, *et al.* (2010) The MetaCyc database of metabolic pathways and enzymes and the BioCyc collection of pathway/genome databases. *Nucl. Acids Res.* 38(suppl_1):D473-479.
69. Schomburg I, Chang A, & Schomburg D (2002) BRENDA, enzyme data and metabolic information. *Nucl. Acids Res.* 30(1):47-49.
70. Herrero A & Flores E (2008) *The cyanobacteria: Molecular Biology, Genomics and Evolution* (Caister Academic Press, Norfolk, UK).
71. Kato K, Tanaka R, Sano S, Tanaka A, & Hosaka H (2010) Identification of a gene essential for protoporphyrinogen IX oxidase activity in the cyanobacterium Synechocystis sp. PCC6803. *Proceedings of the National Academy of Sciences* 107(38):16649-16654.
72. Feist AM, *et al.* (2007) A genome-scale metabolic reconstruction for Escherichia coli K-12 MG1655 that accounts for 1260 ORFs and thermodynamic information. *Mol Syst Biol* 3.
73. Yoo S-H, Spalding MH, & Jane J-l (2002) Characterization of cyanobacterial glycogen isolated from the wild type and from a mutant lacking of branching enzyme. *Carbohydrate Research* 337(21-23):2195-2203.
74. Schledz M, Seidler A, Beyer P, & Neuhaus G (2001) A novel phytyltransferase from Synechocystis sp. PCC 6803 involved in tocopherol biosynthesis. *FEBS Lett* 499:15-20.
75. Nakamura A, Akai M, Yoshida E, Taki T, & Watanabe T (2003) Reversed-phase HPLC determination of chlorophyll a′ and phylloquinone in Photosystem I of oxygenic photosynthetic organisms. *European Journal of Biochemistry* 270(11):2446-2458.
76. Neidhardt FC, Ingraham JL, & Schaechter M (1990) Physiology of the bacterial cell: a molecular approach.
77. Jantaro S, Mäenpää P, Mulo P, & Incharoensakdi A (2003) Content and biosynthesis of polyamines in salt and osmotically stressed cells of Synechocystis sp. PCC 6803. *FEMS Microbiol Lett* 228(1):129-135.
78. Price ND, Reed JL, & Palsson BO (2004) Genome-scale models of microbial cells: evaluating the consequences of constraints. *Nat Rev Microbiol* 2(11):886 - 897.
79. Varma A & Palsson BO (1994) Stoichiometric flux balance models quantitatively predict growth and metabolic by-product secretion in wild-type *Escherichia coli* W3110. *Appl Environ Microbiol* 60(10):3724-3731.
80. Mahadevan R & Schilling CH (2003) The effects of alternate optimal solutions in constraint-based genome-scale metabolic models. *Metabolic Engineering* 5(4):264-276.
81. Becker SA, *et al.* (2007) Quantitative Prediction of Cellular Metabolism with Constraint-based Models: The COBRA Toolbox. *Nat Protoc* 2(3):727 - 738.
82. Rippka R (1988) Isolation and purification of cyanobacteria. *Methods Enzymol* 167:3-27.
83. Ullmann GM, Hauswald M, Jensen A, & Knapp EW (2000) Structural alignment of ferredoxin and flavodoxin based on electrostatic potentials: Implications for their interactions with photosystem I and ferredoxin-NADP reductase. *Proteins* 38:301-309.
84. Matsuo M, Endo T, & Asada K (1998) Properties of the respiratory NAD(P)H dehydrogenase isolated from the cyanobacterium Synechocystis PCC6803. *Plant Cell Physiol* 39:263-267.
85. Becker S, *et al.* (2007) Quantitative Prediction of Cellular Metabolism with Constraint-based Models: The COBRA Toolbox. *Nat Protoc* 2(3):727 - 738.

86. Allen JF (2003) Cyclic, pseudocyclic and noncyclic photophosphorylation: new links in the chain. *Trends Plant Sci* 8(1):15-19.
87. Wingler A, Lea P, WP Q, & Leegood R (2000) Photorespiration: metabolic pathways and their role in stress protection. *Philos Trans R Soc Lond B Biol Sci* 355(1402):1517-1529.
88. Edwards G & Walker D (1983) *C3, C4: mechanisms, and cellular and environmental regulation, of photosynthesis* (Blackwell Scientific publications, Oxford).
89. Kaplan A, Hagemann M, Bauwe H, Kahlon S, & Ogawa T (2008) Carbon Acquisition by Cyanobacteria: Mechanisms, Comparative Genomics, and Evolution. *The Cyanobacteria. Molecular Biology, Genomics and Evolution*, eds Herrero A & Flores E (Caister Academic Press, Norfolk, UK), pp 305-334.